Nanoscale Advances

ROYAL SOCIETY OF CHEMISTRY

REVIEW

View Article Online
View Journal | View Issue

Cite this: *Nanoscale Adv.*, 2020, **2**, 2234

There's no place like real-space: elucidating size-dependent atomic structure of nanomaterials using pair distribution function analysis

Troels Lindahl Christiansen, † Susan R. Cooper † and Kirsten M. Ø. Jensen *

The development of new functional materials builds on an understanding of the intricate relationship between material structure and properties, and structural characterization is a crucial part of materials chemistry. However, elucidating the atomic structure of nanomaterials remains a challenge using conventional diffraction techniques due to the lack of long-range atomic order. Over the past decade, Pair Distribution Function (PDF) analysis of X-ray or neutron total scattering data has become a mature and well-established method capable of giving insight into the atomic structure in nanomaterials. Here, we review the use of PDF analysis and modelling in characterization of a range of different nanomaterials that exhibit unique atomic structure compared to the corresponding bulk materials. A brief introduction to PDF analysis and modelling is given, followed by examples of how essential structural information can be extracted from PDFs using both model-free and advanced modelling methods. We put an emphasis on how the intuitive nature of the PDF can be used for understanding important structural motifs, and on the diversity of applications of PDF analysis to nanostructure problems.

Received 12th February 2020
Accepted 5th May 2020

DOI: 10.1039/d0na00120a

rsc.li/nanoscale-advances

Introduction

When looking back on the developments in materials chemistry over the past decades, it is clear that the discovery and advancement of new functional materials for advanced applications in *e.g.* energy technologies and many other fields has paralleled the ability of scientists to characterize atomic structure in materials.[1,2] The very core of materials chemistry is understanding the relation between atomic structure and properties, and developments in materials chemistry heavily relies on structural knowledge. The ability to determine the atomic structure of materials began with the work of Max Von

Department of Chemistry and Nanoscience Center, University of Copenhagen, 2100 Copenhagen Ø, Denmark. E-mail: kirsten@chem.ku.dk

† These authors contributed equally to this manuscript.

Troels Lindahl Christiansen obtained his Ph.D. degree in Chemistry in 2019 from the University of Copenhagen, working in the nanostructure group under supervision of Kirsten M.Ø. Jensen. He is currently a postdoctoral researcher in the same group. His research focuses on structural characterization of metal oxide materials, as well as on developing new methods for pair distribution function analysis.

Susan R. Cooper received her Ph.D. in Chemistry from the University of Oregon in 2018 (with James E. Hutchison and Darren W. Johnson). She was supported by the National Science Foundation Graduate Research Fellowship program, and her research focused on the synthesis and structural characterization of iron oxide nanocrystals. She is now a Postdoctoral Fellow at the University of Copenhagen, funded by a Marie Sklodwska-Curie Individual Fellowship. Her research is focused on determining the nanoscale structural changes of small nanocrystals using total X-ray scattering and pair distribution function analysis.

Laue and W. H. and W. L. Bragg in the 1910s.[3–5] Epochal developments such as Rietveld refinement[6] and the advent of large scale synchrotron and neutron facilities have allowed materials scientists to tackle structures, materials and problems of ever increasing complexity.[7,8] The result is an explosion in the diversity of the materials we use every day, which has caused a fundamental change in our society and way of life.[9] Still ahead lies challenges to develop cheaper, more sustainable and greener materials with improved properties, tailormade for new technologies. Nanomaterials have the potential to be part of this development and have contributed solutions in a number of important fields.[10,11]

The size-dependent properties observed in many nanomaterials arise from effects including enhanced surface/volume ratio, and for the smallest nanoparticles, quantum confinement effects.[12–14] In addition, the *atomic arrangement* in a material may also change upon nanosizing, which will dramatically influence the material properties. For example, a change of atomic structure is seen in metallic nanoparticles when going below 2–3 nm, leading to completely new properties.[15–18] Despite this, the atomic structure of most nanomaterials is often assumed to be simple cut-outs of the structure of the corresponding bulk materials. This lack of understanding of an important nanoscale effect is most likely due to the difficulty in characterizing atomic structure in nanoscale materials.[19] While the small domain size of the nanomaterials is the origin of emerging properties,[12] it also poses a problem as it challenges the conventional crystallographic methods used for determining and refining the atomic structure of materials.[19,20] In traditional powder X-ray diffraction (PXRD), the Bragg peaks that arise from atomic periodicity in crystalline materials are analyzed to obtain information on the atomic structure of the sample, however this is not sufficient for nanostructured materials, where the crystalline domain size is small and where the structure is often disordered. Consider the standard Rietveld refinement approach:[6] Structural information is extracted by minimizing the difference between experimental PXRD data and Bragg peak intensities and positions calculated from a crystal structure model. Any deviation from perfect crystallinity is included by modelling the Bragg peak shape, which can yield microstructural information such as crystallite size and strain.[21] However, any *diffuse* scattering arising from disorder in the material is normally considered background scattering and conventional Rietveld refinement is often inadequate for structural analysis of nanomaterials whose atomic structure is far from that of bulk, crystalline materials.[22]

Because of the challenges in applying traditional diffraction methods to nanostructured materials, many other techniques have been applied in the quest to characterize their atomic structure.[23] For example, Extended X-ray Absorption Spectroscopy (EXAFS) can be used to characterize the local atomic structure in any material no matter its degree of atomic order, including disordered nanostructured materials.[24] However, the structural information that can be obtained from EXAFS is limited to the first few coordination shells around an atom, making it difficult to fully characterize material structure.[19] Transmission electron microscopy (TEM) is another widely used technique for nanomaterials, and with sufficient resolution, TEM can be applied in the characterization of the atomic structure of nanoparticles.[25–27] However, highly disordered materials can be difficult to characterize from microscopy methods alone and a limited number of particles can be analyzed at a time. Since the turn of the century, X-ray Total Scattering (TS) and Pair Distribution Function (PDF) analysis has been proven to be an extremely powerful technique for the characterization of material structure and has evolved from a method mainly used for characterization of liquids and amorphous matter into a powerful tool for elucidating the atomic structure of solid state materials.[20,28,29] In the early days of PDF analysis of materials, in the late 1990s and early 2000s, the method was an exotic technique applied mainly by solid state physicists to study the local structure in bulk, crystalline materials exhibiting *e.g.* superconductivity or ferroelectricity.[30,31] PDF is still widely used for this type of materials, but since then, the diversity of the applications of PDF has grown tremendously, and PDF is now an important method for structure characterization in chemistry,[32] energy materials,[33–37] geology,[38–40] pharmaceuticals,[41–43] and other fields.

A PDF is a Fourier transform of total scattering data and, as described further below, represents the distribution of all interatomic distances in a material.[22] When treating total scattering data, one does not discriminate between diffuse scattering and Bragg scattering, and the PDF thus includes information on the atomic structure of any kind of material; crystalline, nanostructured, disordered, or fully amorphous.[28] A barrier to wide adoption of the use of PDF in the past was the challenges in measuring high quality scattering data to high momentum transfers, Q, which is needed to obtain high resolution in real-space.[22] Now, the increase in X-ray flux and X-ray energy available at synchrotron sources have made the development of dedicated PDF beamlines possible.[20,22] Combined with developments in experimental methods, such as the rapid-acquisition PDF (RA-PDF) method,[44] and user-friendly software,[45–49] PDF has become a widely accessible technique for a large community of scientists.[31]

Kirsten M. Ø. Jensen is an associate professor at Department of Chemistry at University of Copenhagen. She received her Ph.D. in Chemistry from Aarhus University in 2013. Following a postdoc position at Columbia University, she started her research group in Copenhagen in 2015. The research in her group concerns nanomaterials, focusing especially on the use of X-ray and neutron scattering to elucidate the structure and formation mechanisms of nanoparticles. Pair distribution function analysis is central to her research, and her group is active in development of new PDF modelling methods and experiments.

PDF analysis can now be considered a mature technique capable of characterizing a range of different nanostructures, and its use in several fields has been reviewed in the past.[33,50–54] With this review, we focus on the application of PDF in studies of the size-dependent atomic structure in nanomaterials and aim to give an overview of some of the different approaches that have been applied in studies of nanosize-induced structural changes. We will review examples of PDF studies that use a variety of strategies for data analysis. The PDF method and PDF theory has already been thoroughly reviewed and described in papers and textbooks,[22,55,56] and we therefore only give a short description of the anatomy of a PDF to aid in understanding how structural information can be extracted from total scattering data and PDF analysis before reviewing examples of its use.

Obtaining and reading a PDF

A PDF is obtained by Fourier transforming total scattering data. The Fourier transform is done over the *structure function* S(Q), which represents the normalized, coherently scattered intensity from the sample, as here expressed for X-rays:[22]

$$S(Q) = \frac{I_c(Q) - \left\langle f(Q)^2 \right\rangle + \langle f(Q) \rangle^2}{\langle f(Q) \rangle^2} \quad (1)$$

$$G(r) = \left(\frac{2}{\pi}\right) \int_{Q_{min}}^{Q_{max}} Q(S(Q) - 1)\sin(Qr)\mathrm{d}Q \quad (2)$$

here, $I_c(Q)$ represents the coherent scattering intensity, and $f(Q)$ the atomic form factors for the elements in the sample. Several user-friendly programs, *e.g.* PDFgetX3,[46] PDFgetN,[57] PDFgetN3,[58] GSAS-II,[49] GudrunX and GudrunN[48] can be used to obtain $S(Q)$ and $G(r)$ from experimental total scattering data obtained from X-rays, neutrons or electrons. The extent of the Q-range $\left(Q = \frac{4\pi \sin(\theta)}{\lambda}\right)$ used in the Fourier transform determines the amount of information and detail that can be extracted from the PDF, and generally, a Q_{max} value of at least 15–20 $Å^{-1}$ is needed to extract atomic scale structural information, although this value is highly dependent on the purpose and aim of the study. The need for large Q-ranges means that high energy X-rays or neutrons with a short wavelength should be applied. High flux is furthermore required, as good statistics in the $S(Q)$ function even at the highest Q-values are needed in order to minimize noise in the PDF. In the case of X-rays, total scattering studies are therefore often done at high energy synchrotron sources with dedicated PDF beamlines.[28] However, PDF analysis is also possible with laboratory instruments using *e.g.* Ag or Mo X-ray tubes.[59] Total scattering measurements can also be performed using neutrons[57] or electrons.[60] We focus here on X-rays which is most widely used for nanostructure analysis, but the choice of radiation depends entirely on the sample and scientific aim in question.

A PDF represents the distribution of all interatomic atomic distances present in the structure of a sample. Due to the intuitive nature of the PDF, significant structural insight is

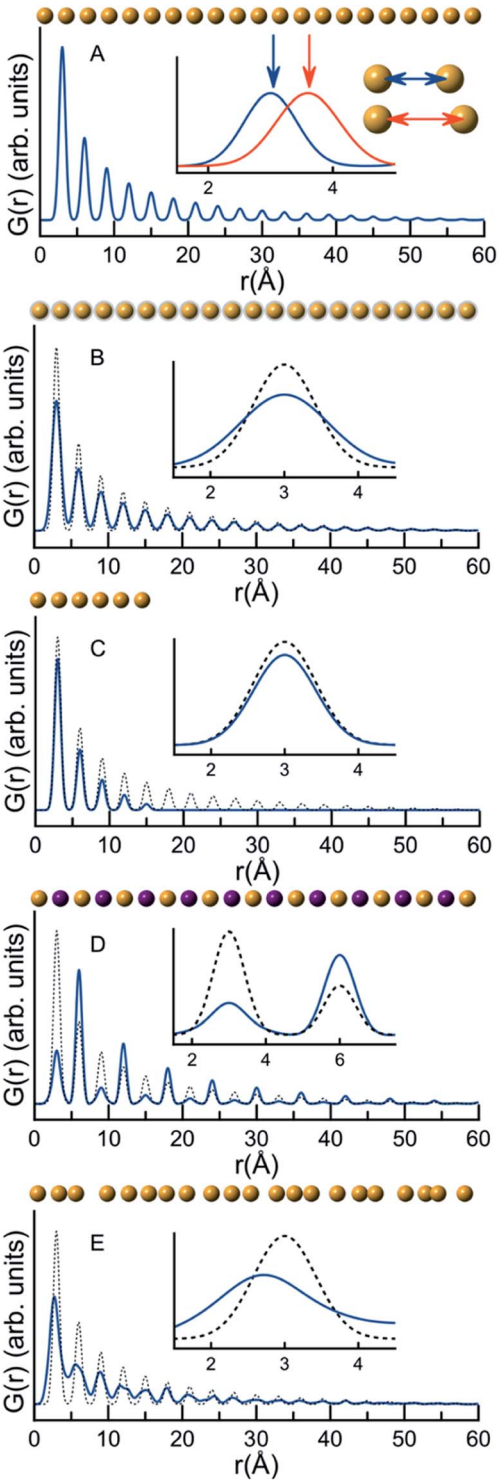

Fig. 1 $G(r)$ functions calculated for hypothetical 1D atomic structures. A–E illustrate different aspects of the PDF and how they are interpreted in relation to atomic structure: (A) the impact of atomic coordinates on peak position, (B) the impact of atomic vibration on peak broadening, (C) the impact of crystallite size on the extent of the PDF, (D) the impact of atomic identity (as seen when replacing Au with Na, an element with lower scattering power) on the peak intensity and (E) the effects of disorder on the PDF. The blue line is the simulated PDF under consideration, while the dotted line is the PDF simulated in A.

available in the PDF from model-free analyses. We show this for a series of very simple, discrete and isolated structures in Fig. 1. In Fig. 1A, a simulated PDF for a hypothetical, one-dimensional structure consisting of a chain of 21 atoms with a bond distance of 3 Å is shown. The first peak in the PDF, at 3 Å, is at the distance between two adjacent atoms; the second peak in the PDF at 6 Å is at the distance between the next pair of atoms, and all subsequent peaks in the PDF follow this same pattern. If the distance between the atoms increases, the peak positions will change as is shown in the insert in Fig. 1A, where the interatomic distance was changed in the simulations to 3.6 Å. The PDF peak width is determined by the distribution of atomic distances for an atom–atom pair. Fig. 1B demonstrates this effect on the PDF in terms of increased thermal vibrations, which increases the PDF peak width. The size of the structure in question also affects the PDF. In Fig. 1C, we show this effect in the $G(r)$ by comparing the PDF simulated from a chain of 6 atoms with that simulated from the chain of 21 equidistant atoms. Lower intensity is observed in the PDF peaks originating from the 6 atom chain compared to the 21 atom chain as fewer atomic pairs are present in the short chain. Furthermore, the intensity of the PDF peaks from the shorter chain diminish quicker with r, and there are no PDF peaks at r values larger than the size of the structure. In studies of nanoparticles, this effect can be used to characterize the size of crystalline domains or crystallite sizes. The PDF peak intensity is proportional to the number of occurrences of an atomic pair; however, the peak intensity is also influenced by the scattering power of the atoms in the pair. Fig. 1D shows a hypothetical structure consisting of two different atoms, Au (gold) and Na (purple). Na ($Z = 11$) has much lower scattering power than Au ($Z = 79$), and peaks originating from atomic pairs involving Na (*i.e.* Na–Na and Na–Au) will therefore have a lower intensity than Au–Au peaks.

The properties of PDFs described above are summarized in eqn (3) and (4), which shows how the PDF can be calculated from a structural model. The Radial Distribution Function (RDF), or $R(r)$ is calculated as the sum of delta functions representing all interatomic distances in the sample, where their weight is given from their (X-ray) scattering power of the atoms in the pair:

$$R(r) = \sum_{v} \sum_{\mu} \frac{f_v f_u}{\langle f^2 \rangle} \delta(r - r_{vu}) \quad (3)$$

A pair of atoms consisting of atoms v and u will give rise to a delta function at r_{vu}, which is the distance between the two atoms. The peak intensity will be given from the scattering power of the two atoms through their form factors f. By summing over all atomic pairs in the sample, the full $R(r)$ is obtained. The $R(r)$ is a member of a large family of pair distribution functions, which all express the same information in slightly different ways as discussed in detail by Keen.[61] The reduced pair distribution function, $G(r)$ illustrated in Fig. 1, is easily obtained from the $R(r)$:

$$G(r) = \frac{R(r)}{r} - 4\pi r \rho_o \quad (4)$$

here, ρ_o is the average atomic number density in the sample. The $G(r)$ function is often used in PDF analysis as this is the function that is directly obtained when Fourier transforming properly corrected experimental total scattering data as seen in eqn (2).

The PDFs illustrated in Fig. 1A–D and discussed above originate from very simple, well-ordered and hypothetical systems. In Fig. 1E, we have tried to simulate effects of disorder in a hypothetical atomic structure by multiplying all atomic positions in the 21 atom 1D chain by a random number. Atomic disorder can influence any and all of the aspects of the PDF discussed above, and thus the PDF peaks in Fig. 1E appear both broadened and shifted due to the disorder. Because all of these simultaneous and inseparable changes affect the features of the PDF, structural disorder is significantly more challenging to model and characterize as will be clear throughout this review when discussing PDFs from real nanomaterials.

Modelling of PDFs

As seen from Fig. 1 and as illustrated in examples below, much structural insight can be obtained from model-free PDF analysis. However, often, modelling of PDFs allow a greater amount and more reliable information to be extracted. Given an atomic structure model, the corresponding PDF can easily be calculated either from a crystal structure or from discrete structural objects such as molecule-like clusters or nanoparticles. The calculated PDFs can then be fitted to experimental data to obtain a refined model for the sample in question by varying the structural parameters.

As we will see throughout the review, several strategies can be applied in modelling PDFs from nanoscale materials of varying complexity. A very widely used approach is the 'real-space Rietveld' method, implemented *e.g.* in the programs PDFgui,[45] DiffPy-CMI[62] and TOPAS.[47] As the name implies, real-space Rietveld refinement is very similar to its namesake in reciprocal space. The structural model is built from a crystallographic unit cell assuming translation symmetry. Variables such as unit cell parameters, fractional atomic coordinates, isotropic or anisotropic atomic displacement parameters (ADPs), and site occupancies can be refined, and most often, the space group symmetry is preserved in the refinements. Effects of crystallite size are usually implemented through an envelope function that dampens the PDF signal as r increases. The envelope function corresponds to a particular particle shape which is usually assumed to be spherical, but can be introduced to reflect many shapes and size distributions.[63,64] While this method is conceptually similar to Q-space Rietveld refinements, modelling the real-space PDF allows analysis of the structure in *e.g.* very small nanoparticles, where the peak broadening challenges conventional Rietveld refinements in Q-space. The local structure and disorder in materials can also be analyzed by *e.g.* fitting r-dependent models that include a separate description of the local structure and the average structure.[65] As many of the examples in the review will show, the applications of real-space Rietveld analysis are incredibly diverse, and with structural insight and creative model construction, this method can be applied to tackle even complex nanostructure analyses.

The real-space Rietveld approach is mostly suited for materials where the atomic structure shows periodicity and is related to the crystal structure of the corresponding bulk material or other known crystalline structures. In many materials, containing *e.g.* molecular units, large ionic clusters, or metallic nanoclusters, this approach cannot be used to describe the atomic structure. PDF modelling can then be done without assuming translation symmetry and periodicity, *i.e.* by building up a discrete structural object through its atomic coordinates. This method, used for small nanoparticles, clusters and molecules, takes advantage of the Debye equation[66] for calculation of a scattering pattern and subsequently the PDF.[67] In the case of nanoparticles, an entire structural model can be built and fitted to the data. Software packages such as DISCUS[68] and DiffpyCMI[62] facilitate modelling of PDFs of discrete structures. Analysis of scattering patterns using the Debye scattering equation can also be done directly in Q-space, *i.e.* without Fourier transforming the data,[69] for example using the *Debussy* program.[70] Unlike in Q-space or real-space Rietveld analysis, where the space group symmetry can be applied to constrain the parameters in the refinements, extra care has to be taken in limiting the number of refinable parameters when fitting discrete models. However, as examples below will show, this approach can be extremely powerful for structural analysis of small nanoparticles.

PDF analysis can also be done using 'large-box modelling', *e.g.* through the use of Reverse Monte Carlo (RMC) methods, where thousands of atoms in a structure are allowed to move to better fit experimental PDFs.[71–73] While widely applied for fully amorphous and disordered crystalline materials, this approach has been less used for nanomaterials, although recent examples have shown its application to nanoparticles.[74–76]

Independent of the approach to modelling, the quality of a fit to a PDF is often analyzed through the R_w-factor, which is a measure of the difference between the calculated (G_{calc}) and experimental PDF (G_{obs}) that is calculated as:[22]

$$R_w = \sqrt{\frac{\sum_n (G_{obs,n} - G_{calc,n})^2}{\sum_n {G_{obs,n}}^2}} \quad (5)$$

It is difficult to establish exactly what the R_w value for a 'good' fit should be. PDF is often used to characterize very different materials with varying degrees of structural order, and the R_w-value that can be expected depends greatly on the structure type investigated as well as the data quality. When fitting high quality PDFs from highly ordered, crystalline models, very good agreement between data and model can often be obtained with R_w values between 1–5%. This is rarely the case for nanostructured and disordered materials, where satisfactory fits are reported with R_w values above 15%. Often, the complexity of a disordered nanomaterial is too high for a relatively simple model to fully describe *e.g.* heterogeneous size and structure. The quest for a good fit is always a compromise between extending the number of parameters in the model (which may result in over-fitting and unphysical models) and the development of simple models that describe important structural features in the sample. A visual inspection of the fit is key when evaluating the fit quality, as large features in the difference curve are clear indications of an inadequate structure model. Due to the intuitive nature of a PDF, features in the difference curve can often be directly linked to a structure motif, which can aid in developing better models, as discussed further below.

Nanostructure from PDF analysis

In the following, we will review examples of the use of PDF for analysis of atomic structure in nanomaterials. This is a large and quickly developing field, spanning over a range of material types, applications, experimental methods and approaches to structure analysis. We do not aim to cover the whole field, but we have chosen examples applying different analysis methods to the structures that appear on the nanoscale; from model-free analysis, to real-space Rietveld refinements, and discrete cluster modelling of varying complexity. The examples range from early applications of PDF for nanoparticle studies to recent examples of its use. As will be seen from the diverse examples, the method to be used for a specific study is highly dependent on the problem that is under investigation, and what information is sought. This means that PDF analysis of the atomic structure in nanomaterials requires a great deal of creativity, structural understanding and chemical intuition. We have divided the examples into three material classes; metal chalcogenides, metallic nanoparticles and oxides, and in this way, we try to cover a broad range of materials as well as approaches for PDF analysis.

Size-dependent structure of metal chalcogenide nanoparticles from PDF analysis

Stacking faults and size-dependent structure in metal chalcogenide nanoparticles. Layered metal chalcogenides such as $LiMoS_2$ (ref. 77) and WS_2 (ref. 78) provided early examples of the PDF technique applied to *crystallographically challenged* nanostructured materials,[50,55] and since then, the structure of several chalcogenide nanomaterials have been characterized with PDF.[79–82] Many metal chalcogenide nanoparticles are of particular interest because of their photoabsorptive properties, and because of the extraordinary synthesis-control that can be achieved over both size and structure.[83] The band gap of metal chalcogenides can be tuned both with nanosizing and by changing the chemical composition of the material,[84] and it is therefore crucial to elucidate the size- and composition-dependent structure of these materials. For example, ZnS (one of the first semiconductors ever discovered) has been reported to have size-dependent electronic properties making it an interesting material for structural studies. Furthermore, the synthetic size control possible for *e.g.* CdSe[83,85] made these types of materials an early target for PDF studies of size-dependent nanostructures. Bulk ZnS and CdSe crystallize in either the wurtzite or zinc-blende (sphalerite) structure. The two structures have identical closed packed layers, but they differ in their stacking sequence; hexagonal wurtzite shows ABABAB stacking,

and cubic zinc-blende ABCABC stacking as shown in Fig. 2. Both structures are prone to stacking faults which affect the material properties, and the presence of stacking faults is highly dependent on the size of the particles.[86]

In small particles of CdSe it has been difficult to distinguish between the zinc-blende and wurtzite phases using conventional diffraction and microscopy techniques.[87,88] Using PDF, Masadeh *et al.*[86] fitted structural models (using the real-space Rietveld approach) of both phases to the PDF of bulk CdSe and nanoparticles with approximate sizes of 3.5 nm (III), *ca.* 2.9 nm (II) and 2.0 nm (I). The fits revealed unphysically large ADPs that increase with decreasing particle size. In the wurtzite fit, anisotropic ADPs were applied, and they showed increased values along the stacking direction in the unit cell *i.e.* along the *z*-axis. The increased ADPs in the stacking direction were interpreted to indicate the presence of stacking faults, and the increase in ADPs with decreasing particle size could therefore be interpreted as an increase in stacking fault density. To test this hypotheses, the authors built CdSe nanoparticle models with different stacking fault densities using the DISCUS[68] program, and PDFs of the different structures were simulated applying fixed, isotropic ADP values. The simulated PDFs were subsequently fit using a wurtzite model with anisotropic ADPs, *i.e.* using the same approach as for the experimental data. Again, the refined ADPs from the simulated data were unphysically large in the stacking direction due to the stacking faults introduced in the models. However, the refined ADP values along the stacking direction could now be directly correlated to the specific stacking fault density introduced in the constructed models. Using this information, the stacking fault density in the samples were determined to be *ca.* 35% in bulk CdSe and 50% in the nanoparticles. The experimental PDFs were then fit with structural models with the appropriate stacking fault density, which yielded excellent fits with physically reasonable ADP values.

In a later paper, Yang *et al.*[89] applied the real-space Rietveld approach to extract approximate stacking densities in similar CdSe nanoparticles, using two-phase models. In Fig. 3, real-space Rietveld refinements of a CdSe nanoparticle PDF are shown using a zinc-blende model (top), a wurtzite model (middle) or a two-phase model using both structures (bottom). Only the two-phase model is able to correctly describe all positions and the intensity of the PDF peaks. The authors recognized that the PDFs of wurtzite and zinc-blende would be identical for the first two stacking layers (AB) but would differ in the third layer (A or C). They defined a stacking fault density with regards to wurtzite as P(C), which is the probability of a C-layer occurring in third position of the stacking sequence. Thus, for wurtzite P(C) = 0 (no C in third layer), while P(C) = 1 (C always in third layer) corresponds to the zinc-blende structure. A wurtzite structure with stacking faults would have a P(C) between 0 and 1. In the study, P(C) was approximated by refining the phase fraction between wurtzite and zinc-blende in a limited *r*-range of the PDF that only includes the first three layers (1–10 Å). The mixed phase models showed an excellent agreement with the data of the nanoparticles, except for the PDF from ultra-small CdSe particles (*ca.* 1.3 nm), which appear to have a different atomic structure to the other particles that was not elucidated from the broad and dampened PDF peaks. Consistent with the previous study, the stacking fault density is seen to increase with decreasing particle size from *ca.* 8% in the bulk sample to *ca.* 30% in the small nanoparticles. The correct stacking sequence after the third layer of stacking is not described in a two-phase real-space Rietveld model, however, the advantage of this approach is the ease and computational speed by which it can be applied to extract stacking fault densities.

Both papers on the structure of CdSe nanoparticles (Masadeh *et al.*[86] and Yang *et al.*[89]) also demonstrate how model-free analysis can allow information to be extracted from PDF. By simply observing the changes in the width and position of the first Cd–Se peak in the PDFs, it is possible to extract information

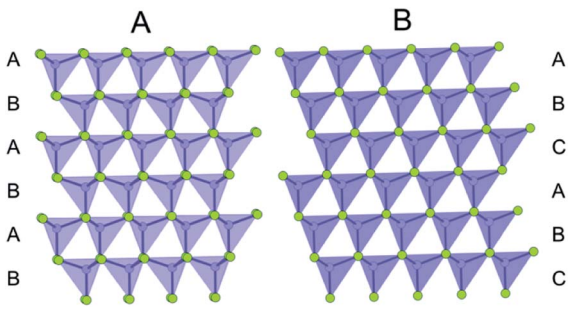

Fig. 2 Illustration of the stacking sequence in the wurtzite structure (A) and the zinc-blende structure (B). Cations are represented as purple dots, and anions are represented as green dots. The tetrahedrally coordinated Cd cations are shown to emphasize the layering of the structure.

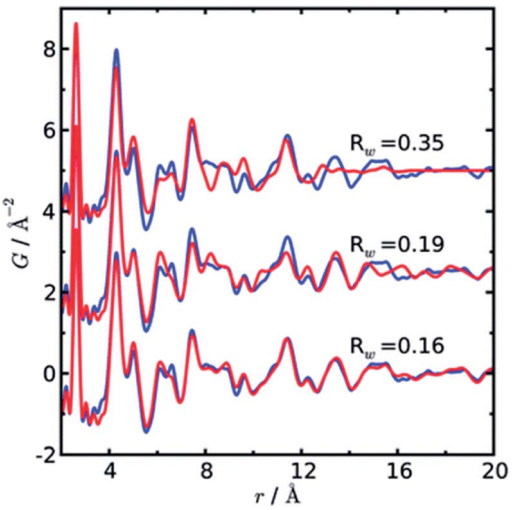

Fig. 3 Three real-space Rietveld refinements of a PDF from CdSe nanoparticles (3.5 nm). The PDF is fit using a zinc-blende model (top), a wurtzite model (middle) or a two-phase model using both structures (bottom). The blue line is experimental data and the red line is a simulated PDF. Reproduced from Yang *et al.*, *Phys. Chem. Chem. Phys.*, 2013, **15**, 8480–8486 (ref. 89) with permission from the PCCP Owner Societies.

on the strain in the particles. Homogeneous strain will cause a shift in all bond-lengths, which causes the position of the peak in the PDF to move, while inhomogeneous strain causes broadening of the peak due to a non-uniform distribution of bond-lengths. The width and position can be extracted by fitting *e.g.* a Gaussian function to the peak, as seen in Fig. 4a. The resultant changes in position and width is shown as a function of particle size in Fig. 4b and c, respectively. From the figures it is evident that both the homogenous (position) and inhomogenous (width) strain increase rapidly with decreasing particle size, consistent with the increase in structural disorder and the presence of stacking faults evident from the modelling.

While the intuitive nature of PDF can facilitate the description of defects and stacking faults, it should be noted that stacking faults and other defects in metal chalcogenides are also often studied in *Q*-space analysis of total scattering data,[90–92] or in a combination of *Q*- and *r*-space refinements.[93,94] For example, Mosheni *et al.* used the Debye equation in a complex and highly advanced analysis of small and wide angle X-ray scattering data to determine stacking faults and faceting in CdSe nanoparticles.[95] Niederdraenk *et al.* used ensemble modelling to determine distributions of stacking faults, sizes and morphologies of small CdSe, ZnS and ZnO nanoparticles.[96,97]

Other chalchogenide nanoparticles crystallize in the rock salt structure, where PDF and other scattering methods have been applied to study structural distortions from the ideal lattice in the bulk.[98] Studies of nanoparticles using total scattering methods have revealed size-dependent structural distortions,[99] and PDF and a suite of nanoscale characterization techniques have been applied to study nanoparticles in the $Pb_mSb_{2n}Te_{m+3n}$ system, where compositions that do not have stable bulk counterparts can be synthesized as nanomaterials.[35]

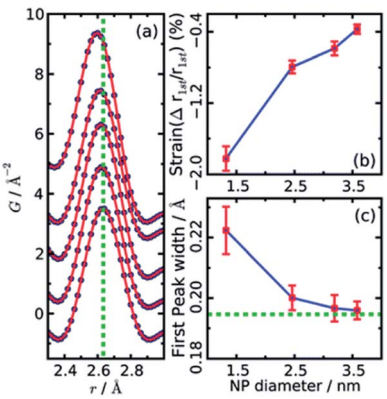

Fig. 4 (a) Gaussian fits to the first peak in experimental PDFs of CdSe nanoparticles of various sizes. Data are represented as black dots, and the fit as a red line. The green dotted line indicates the peak *r* value from a bulk sample. (b) The relative percentage change in position as obtained from the Gaussian fits, plotted as function of nanoparticle size. (c) Changes in peak width obtained from the Gaussian fits, plotted as function of nanoparticle size. The green dotted line indicates the value of peak width from a bulk sample. Reproduced from Yang *et al.*, *Phys. Chem. Chem. Phys.*, 2013, 15, 8480–8486 (ref. 89) with permission from the PCCP Owner Societies.

Magic-sized metal chalcogenide nanoclusters. In recent years, synthetic control in chalcogenide chemistry has allowed not only the synthesis of highly size controlled nanoparticles, but even of atomically monodisperse 'magic-sized' nanoclusters.[85,100] For magic-sized clusters it is often possible to crystallize diffraction-quality single crystals and solve the structure using single-crystal X-ray diffraction. For example, 3 different 'magic-sized' CdSe nanoclusters were recently synthesized by Beecher *et al.*,[101] containing 35, 56 and 84 Cd atoms. Single crystal diffraction was applied to determine the pyramidal tetrahedron structure of the smallest CdSe cluster. However, two larger CdSe clusters did not form single crystals, and instead PDF was used to characterize the cluster structures. Using the Debye approach to PDF analysis, where discrete structural objects are constructed, excellent fits of the PDF were obtained by adding additional layers to the CdSe tetrahedrons to fit the larger clusters. This model supports the suggested "quantized" layer-by-layer growth. In a study by Stein *et al.*,[102] PDF was used to investigate the structural transitions occurring in $In_{37}P_{20}$ magic sized clusters upon cation exchange with Cd. Using PDF, the existence of 3 structurally different magic sized clusters were demonstrated, including a partially substituted In–Cd–P cluster that is isostructural to the CdSe pyramidal tetrahedron. The studies of magic-sized chalcogenide clusters use discrete, non-periodic objects as models, where the Debye equation is used to calculate the scattering intensity and PDF from the structure. From these studies, it is clear that a good starting model for structure is needed in the analysis, *e.g.* from related single crystal experiments, theoretical predictions, or other characterization methods.[103]

Characterization of strain and surface effects in metal chalcogenide nanoparticles. Detailed studies on strain in chalcogenide nanoparticles using PDF was done by Gilbert *et al.*,[104] who studied the structure of ZnS nanoparticles using PDF in combination with high resolution transmission electron microscopy (HR-TEM), small angle X-ray scattering (SAXS) and EXAFS in order to characterize the 'stiffness' of the nanoparticle structure. In Fig. 5A, the experimental PDF of 3.4 nm ZnS nanoparticles (size determined from TEM and SAXS) is compared to a PDF calculated from a bulk zinc-blende (sphalerite) model and a PDF calculated from a truncated 3.4 nm zinc-blende nanoparticle model. The peaks in the experimental PDF are significantly broader and are shifted in *r* compared to the bulk zinc-blende PDF. The experimental PDF also dampens with *r* much faster than would be expected for the 3.4 nm size, as seen in Fig. 5A when comparing the data to the calculated PDF from the nanoparticle model. The broad peaks and the fast damping are clear indications of disorder in the atomic structure of the zinc-blende nanoparticles. However, as illustrated in Fig. 1B, broadening of PDF peaks is also caused by thermal atomic vibrations, and the two contributions to broadening must be distinguished in order to quantify disorder. To separate the static disorder from thermal vibration, the thermal parameters were refined for a PDF from data measured for a bulk ZnS sample, and it was then assumed that the thermal contribution in the bulk and nanostructured sample was

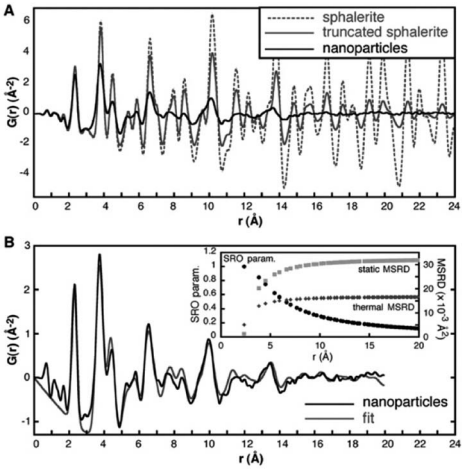

Fig. 5 (A) Experimental PDF of ZnS nanoparticles (black line) compared to a simulated PDF from a 3.4 nm ZnS particle with a zinc-blende structure (grey line) and a simulated PDF from bulk zinc-blende (dashed line). (B) Fit (grey line) to the experimental PDF of ZnS nanoparticles (black line), taking into account particle size and using atomic displacement parameters (MSRD) from a bulk ZnS sample. The *r* dependence of the additional mean square displacement parameter and the short-range order parameter included in the model is shown in the insert. Reproduced from Gilbert *et al.*, *Science*, 2004, **305**, 651–654.[104] Reprinted with permission from AAAS.

identical. The refined bulk thermal parameters were included in the model of the ZnS nanoparticles without further refinement. Any additional broadening of the PDF peaks was then assigned to disorder in the nanoparticles, and an excellent model of the ZnS nanoparticle could be obtained by introducing two different disorder parameters; a static, mean squared relative displacement (MSRD) parameter, and a short-range order (SRO) parameter. The *r*-dependence of the two parameters are shown in the insert in Fig. 5B. The MSRD broadening to the PDF peaks shows approximately the same *r*-dependence as the thermal disorder, where increased broadening is seen with higher *r* due to correlated motion of neighboring atoms. The short-range order (SRO) parameter quenches the PDF intensity at high *r* values due to an increased deviation from the crystallographically expected atomic position with *r*, which is the cause of the more rapid termination of the ZnS nanoparticle PDF compared to the calculated truncated model. The SRO-parameter is associated with strain; however, the authors note that the strain behavior cannot be described by any simple, known strain model. The hypothesized cause of the strain is related to the particle interface with the environment at the surface of the particle. This is expected to force structural rearrangements of the atoms close to the surface, which permeate through to the core of the nanoparticle. As observed in the PDF, these rearrangements cause significant structural disorder in small nanoparticles.[104]

PDF analysis has also been used to determine the structural effects of changing the environment surrounding nanoparticles, *e.g.* the effect of ligands, solvent, or the atmosphere.[103,105–107] For example, Zhang *et al.* studied the dependence of the atomic structure on hydration in 3 nm ZnS particles.[108] The particles were synthesized in anhydrous methanol, and using PDF analysis, it was found that the as-synthesized nanoparticles were highly disordered as reflected by the less than 1 nm coherent scattering domain seen from the PDF. However, when water was added to the particles, a stabilization of the surface occurred, and the atomic structure of the particles became much more ordered. The PDF clearly showed an increase in the size of the coherently scattering domain as could be deduced from peaks at higher *r*-positions in the PDF. Here, disordered particle atomic models were constructed using molecular dynamics simulations by relaxing various sizes of ZnS particles with and without water on the surface. Models were found that fit well with the experimental PDFs and the simulations showed that the surface restructuring in the non-passivated particles penetrated approximately 0.8 nm, leaving only a very small crystalline particle core unperturbed.

Size-dependent structure in metallic nanoparticles

Metal nanoparticles have many important technological applications that often rely on properties unlocked at the nanoscale.[109,110] For instance, gold is a noble metal in bulk form, but when reduced to the nanoscale it exhibits size-dependent tunable catalytic behavior.[111] The existence of a size-dependent structural change from the fcc structure, seen in bulk metals, to a non-fcc structure within small metallic nanoparticles has long been known from studies using HR-TEM and PXRD,[15,112–114] where the presence of *e.g.* decahedral and icosahedral structures were observed. Icosahedral and decahedral structures are shown in Fig. 6C and D, along with an fcc (A) and a tetrahedrally close packed (tcp) Frank–Casper phase (B)[115,116] that will be discussed further below. The decahedral and icosahedral structures contain multiple twinned fcc regions that make up discrete particles that express different surfaces

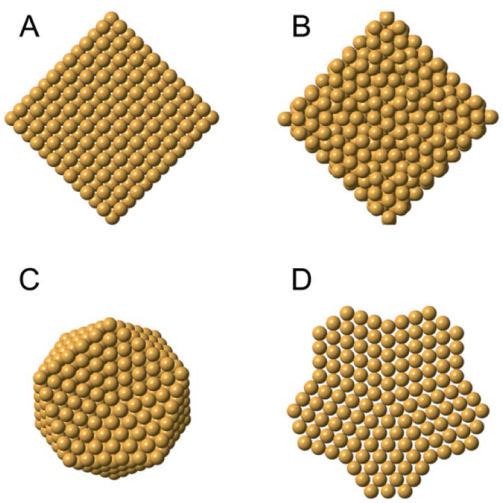

Fig. 6 Different structures seen in metal nanoparticles. (A) The face-centered cubic (fcc) structure; (B) the tetrahedrally close-packed (tcp) Frank–Casper phase, (C) a 561-atom icosahedral cluster core, and (D) an 811-atom decahedral cluster core. The structures in C and D are generated using the ASE module.[122].

and internal atomic structure.[117–119] PDF is a useful technique to characterize such structures[120,121] and early studies helped to demonstrate the ability of PDF analysis to elucidate nanostructure before the technique was widely used in the materials chemistry communities.

Non-fcc structures in metallic nanoparticles. An early study of non-fcc structures in metal nanoparticles was done by Petkov *et al.*,[121] who studied the structure of 30, 15 and 3 nm Au particles, as well as bulk Au. The presence of significant structural disorder could be deduced from the PDF by considering the width of the first Au–Au peak as well as the damping of the PDFs. The width in the PDFs of the nanoparticles reflected a much broader distribution of nearest neighbor distances than in the bulk structure, which is interpreted as a local structure defect. The PDFs of the nanoparticles were modelled using an fcc structure, and fairly good fits were obtained for the PDFs of 30 nm and 15 nm particles, while the PDF of the 3 nm particles shows significant discrepancies between the data and the model, and the structure of the 3 nm gold nanoparticles can no longer be considered fcc. To model this nanostructure, the authors found multiple lowest energy configurations of the 3 nm nanoparticles using Monte Carlo simulations of a 2000 Au atom cluster decorated with 3000 H_2O molecules as ligands, and the most probable models were determined by comparison with the experimental PDF. They found that the 3 nm particles were characterized by extended structural defects and differently oriented domains of fcc within the nanoparticle.

Since then, several PDF and total scattering studies have focused on the structures of non-fcc and hcp structures in metallic nanoparticles.[117,123,124] Vargas *et al.* used PDF and TEM to characterize the atomic structure in long and ultrathin Au nanowires. In this study, many possible structural models in 2 nm by 12 nm nanowires were generated and energetically optimized using Molecular Dynamics simulations. The models tested included structural models that are adopted by bulk gold (fcc and hcp structures), models previously observed in gold nanowires (Boerdijk–Coxeter–Bernal helix, spirals and attached gold nanoparticles) and models from other bulk metals (α-Mn, β-Mn and β-W). For the models that most closely resembled the PDFs obtained from the synthesized nanowires, RMC refinements were performed. It was found that α-Mn, which closely resembles a tcp structure, provided the best fit to the data.[76,125] The nanowires are formed from particle assembly in solution and it was suggested that they adapt the tcp-like structure in order to maintain close atomic packing while avoiding the strain introduced by the high surface area of the nanowires.

Recently, Banerjee *et al.*[126] did a comprehensive study of a range of different metallic nanoparticles, including Pt, Pd, Au and alloys such as CoPd and PtRu. The study puts a large emphasis on scrutinizing the fit residual, and Fig. 7 shows the fit residual obtained when fitting a range of different metal nanoparticle PDFs with an fcc model using the real-space Rietveld approach. The residual from the fit of a bulk Ni standard with an fcc Ni model is seen at the bottom of the figure and is essentially a flat line with small fluctuations mostly due to noise in the data. In comparison, the fit residuals of all investigated nanoparticles show large distinct features. Features

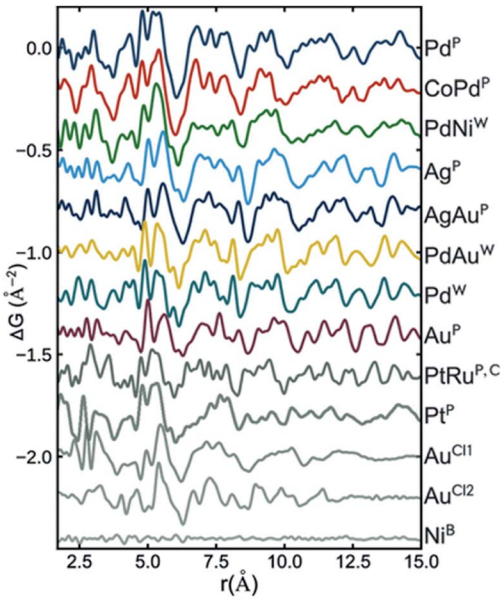

Fig. 7 Fit residuals from real-space Rietveld refinements using an fcc model to several experimental PDFs of different metallic nanoparticles. The difference curve has been scaled for easier visual comparison. Reprinted with permission from Banerjee *et al.*, *J. Phys. Chem. C*, 2018, **122**, 29498–29506.[126] Copyright 2018 American Chemical Society.

exhibited in the fit residual is an indication that the applied fcc model is insufficiently describing the structural information available in the PDF, and the authors proceed to show that a discrete decahedral nanoparticle model significantly reduces the fit residual in comparison with the fcc model. Nanoparticle models with similar particle shape, but without the presence of twin domains were compared to decahedral models, and generally resulted in poorer fits of the experimental PDFs. This shows that the PDFs reflect an actual rearrangement at the atomic level that can be described by twinned domains of an fcc structure rather than an effect of the morphology of the nanoparticles. The decahedrally twinned cluster cores were observed in a majority of nanoparticles used in the study, and the authors point out that including this nanostructure in models of metallic nanoparticles should take precedent over employing complex surface rearrangements or ligand interactions.

In an innovative approach to structural characterization of metallic nanoparticles, Banerjee *et al.* have moved on to show that the identification of metallic cores can be done in an automated manner.[127] The configurations of the different cluster cores such as icosahedral and decahedral structures are well-known, and software packages such as ASE[122] can be applied to build nanoparticles of different sizes, shapes and geometries. The authors generated a large number of discrete nanoparticles, ranging in size from tens of atoms to around 1500 atoms with different geometries and subsequently fit all of them to an experimental PDF of Pd nanoparticles. Fig. 8 illustrates the fit quality (R_w) as a function of number of atoms for a range of different structure types. The R_w value obtained in a real-space Rietveld fit using an fcc structure is given as the green circle with the letters AC (attenuated crystal). The cluster-

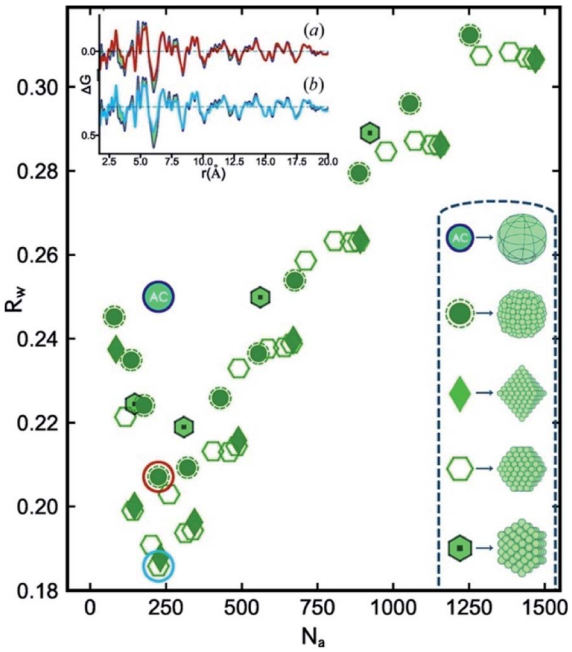

Fig. 8 R_w values obtained for a number of discrete non-twinned nanoparticle models, fitted to the experimental PDF of Pd nanoparticles. The R_w values are plotted as a function of the number of atoms in the structure. The teal circle labelled AC corresponds to the R_w obtained from a real-space Rietveld refinement of the data using an fcc model. Symbols for the discrete nanoparticle models with different geometries can be seen in the bottom right of the figure. Figure from Banerjee *et al., Acta Crystallogr., Sect. A: Found. Adv.*, 2020, **76**, 24–31.[127]

screening process reveals that several of the discrete nanoparticle models yield significantly lower R_w values when fit to the experimental PDF. Initially, fcc-based structures without twinning were tested, and the best model found from this initial cluster-screening is a cuboctahedron with 225 atoms. However, the difference curve in the insert of Fig. 8 reveals significant features similar to those shown in Fig. 7, and therefore, the cuboctahedron model is not fully describing the Pd nanoparticle structure, due to the lack of a twinned cluster core. When also considering twinned cluster cores such as icosahedral and decahedral models in the structure search the R_w value are further improved, and the best model found is a 609 atom decahedron. The decahedron is nearly twice as large as the cuboctahedron model found in the initial search. The decahedron nanoparticle model has a diameter of *ca.* 3.6 nm, which is much closer to the TEM estimate of 3.0 ± 0.3 nm than the cuboctahedron model. The reason for this is that the size initially extracted from the PDF reflects the size of the coherently diffracting twinned fcc unit in the structure, and not the physical size of the particles as seen in TEM. The size of the fcc unit in a 3.6 nm decahedron particle is approximately 2 nm, which explains the small size obtained when applying the non-twinned fcc models. This further demonstrates the importance of determining the correct cluster core when extracting structural information from PDF. In general, large discrepancies between the physical size (TEM, SAXS) and the size of the coherently scattering domain (PDF, PXRD) can be used as an indication of the presence of nanostructure which then must be included in a structural model, as is also discussed for the ZnS particles above.

The novel method of algorithmically generating clusters and automatically screening them for their potential to fit experimental PDFs is promising, as it greatly increases the number of models that can be assessed, as well as reducing human selection bias in the model. If the results from the structure-screening are properly scrutinized, the method has the potential to greatly aid in the characterization of nanomaterials. For instance, we have recently applied a similar method to disordered MoO_x nanostructures supported on alumina and zeolite particles. In this study, a large number of possible models were algorithmically generated and used to extract information on the average structural motifs from the best models discovered.[128]

An even more pronounced structural rearrangement from the common fcc structure has been observed for NiPd alloy nanoparticles in a study by Doan-Nguyen *et al.*[129] Here, TEM was used to demonstrate a very high uniformity of particle size in the synthesized particles as shown in Fig. 9b. From the corresponding PDFs in Fig. 9a, it is readily apparent that significant changes in atomic structure occurs below 5 nm. The PDFs of the particles larger than 5 nm display distinct peaks that can be modelled reasonably well using an fcc model in the real-space Rietveld approach. However, for the 5 nm particles, the much broader PDF peaks signify a large degree of structural disorder. The PDF could not be modelled using the same fcc model, and in fact the signal in the experimental PDF is out-of-phase with the fcc model due to a very different distribution of atoms in the model and PDF. The PDFs could be modelled using an icosahedral core model with very high ADPs to encompass the large structural disorder, and the authors note that the PDF is very

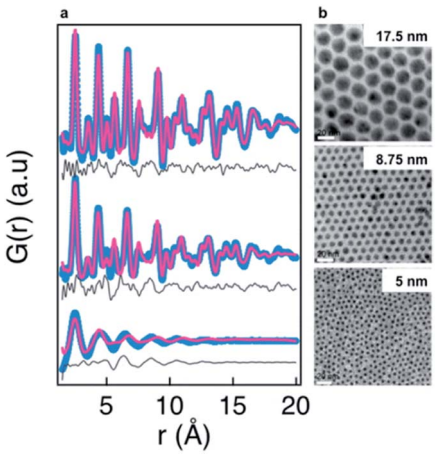

Fig. 9 Characterization of three NiPd samples using PDF and TEM. (a) Fits of PDFs using an fcc structure. The experimental PDF is shown in blue, the calculated PDF in red, and difference curve in grey. (b) TEM images obtained for the three NiPd samples, scale bar is 20 nm. Reprinted with permission from Doan-Nguyen *et al.*, *ACS Nano*, 2014, **8**, 6163–6170.[129] Copyright 2014 American Chemical Society.

similar to that found from bulk-metallic glasses. The model used to fit the data for the <5 nm particle provides a reasonable fit of the PDF data; however, the interpretation of the model is somewhat difficult, and the authors also show that the PDF signal is close to a damped sinusoidal wave. This is a ubiquitous challenge in PDF studies of highly disordered materials.[89,128,130,131] In the case of highly disordered materials, atomic structure cannot be determined with the same specificity presented previously. Instead, as is discussed in the PDF literature available on bulk metallic glasses[132] or liquids,[133] information about the degree of structural order/disorder and the possible local structural motifs can be elucidated.

Magic-sized metallic clusters. Magic-sized clusters, as introduced in the discussion of chalcogenide systems, can also be synthesized for a range of metallic nanoclusters.[17,134,135] Some atomically precise magic number gold clusters can be crystallized into large crystals and thereby be characterized by single crystal X-ray diffraction,[136] however, many other magic number clusters have been predicted and synthesized[137] that are too large to be crystallized. For such systems, PDF has been used in a suite of techniques to determine their structure.[138,139] For example, magic-sized thiol stabilized $Au_{144}(SR)_{60}$ clusters were studied using PDF, where it was demonstrated that the different decahedral and icosahedral core-structures characteristic of metallic nanoparticles can be resolved using PDF by Debye equation based modelling of discrete structures.[140] The experimental PDFs of the gold clusters stabilized using two different ligands (Fig. 10a and b) were significantly different, revealing distinct atomic structures. The PDFs were modelled from discrete models using the Debye equation. The experimental PDF from hexathiol (SC6) stabilized particles shown in Fig. 10a could be fit using an icosahedral structural model previously suggested.[141] However, this icosahedral model provided a poor description of the peaks beyond the nearest-neighbor Au–Au peak in the PDF obtained from clusters stabilized with *para*-mercaptobenzoic acid (*p*-MBA), as shown in Fig. 5B, and evidently the particle core atomic packing must be different. A two-phase model using fcc and hcp atomic gold structures provided an improved fit as shown in Fig. 10c, which indicated that stacking faults or twinning exists in the particles.[124] This 2-phase model mimics stacking faults in metallic systems, but it did not give a physical description of the $Au_{144}(SR)_{60}$ clusters. A model containing a decahedrally twinned core decorated with S–Au–S 'staples' was subsequently constructed by considering information from previous studies of gold cluster structures using techniques complimentary to PDF. The model provided an excellent description of the data, including the small Au–S peak at *ca.* 2.8 Å as shown in Fig. 10e. Thus, both decahedral and icosahedral cores were observed for Au nanoparticles using different stabilizing ligands. Unexpectedly, with other thiol ligands, the two cores were observed to coexist within the sample, which showed that the two core arrangements must be very close in energy.

Supported metal nanoclusters for catalysis: d-PDF studies. In heterogeneous catalysis, catalytic metal nanoparticles are often dispersed on high-surface area supports that save active material, prevent their agglomeration, and potentially improve

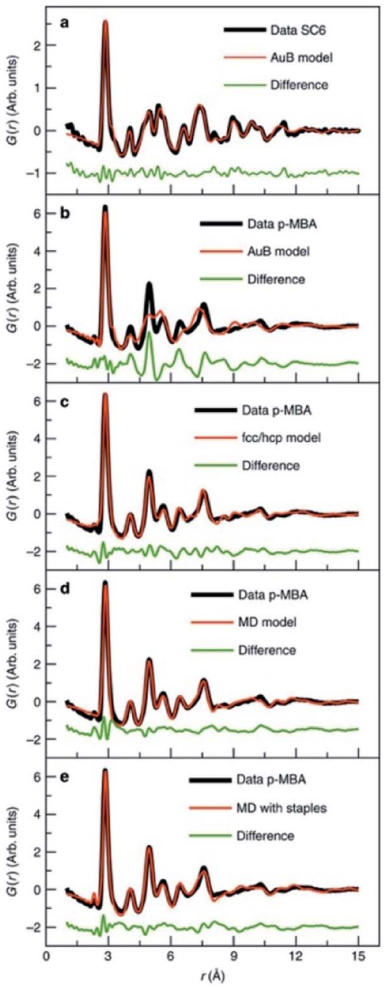

Fig. 10 Fits to experimental PDFs from $Au_{144}(SR)_{60}$ samples. (a) Fit of an icosahedral structure model to data collected from $Au_{144}(SC)_{60}$. (b) Fit of an icosahedral structure model, (c) of an fcc/hcp model, (d) a 114 atom decahedral model and (e) a decahedral model with 'staples' to the PDF obtained from $Au_{144}(p\text{-MBA})_{60}$. From Jensen *et al.*, *Nat. Commun.*, 2016, **7**, 11859.[140]

catalytic performance.[142–144] Typically, the supports are loaded with 1–15 wt% of metallic nanoparticles. When collecting total scattering data from a supported sample, the signal is generally dominated by the support material. One way to bypass this problem is by calculating the so-called difference PDF (d-PDF)[145,146] by measuring a PDF of the support with and without nanoparticles on the surface, and subtracting the first from the latter. In this way, a PDF containing only the signal associated with the supported nanoparticles is obtained. This method can then be used to study *e.g.* the structure of the active catalysts and structural changes occurring under catalysis, which is critical for optimizing catalyst performance.[147–150] For example, Lei *et al.* studied the structural changes occurring when supported platinum nanoparticles adsorbed different small molecules during catalytic reactions.[151] The PDF measurements were performed in a gas flow cell, where atmosphere and temperature can be controlled. The platinum nanoparticle surface was cleaned by heating in a H_2/He mixture, and total scattering data

were collected as the clean particles were exposed to He, H_2 and CO in sequence. PDF analysis showed a clear structural response to the exposure of different gases, especially in the smallest 1 nm nanoparticles. For example, it was found that the 'clean' nanoparticles in He showed a Pt–Pt bond distance of 2.74 Å, which is a 1.4% contraction from the bulk Pt–Pt distance in 2.78 Å, an effect which has been seen in several other studies of platinum nanoparticles.[152,153] However, in H_2/He and CO/He atmospheres, where either H_2 or CO is adsorbed on the surface of the nanoparticles, the Pt–Pt bond relaxed back to 2.77 Å and 2.78 Å, respectively. The structural disorder in the particle was estimated based on the FWHM of the first Pt–Pt peak in the d-PDFs. The FWHM decreased with the adsorption of CO and H_2 revealing that the adsorption enhances the crystallinity of the Pt particles. The bond contraction and poorer crystallinity in clean Pt nanoparticles were suggested to be due to the under-coordination of the Pt atoms on the surface of the particles. The adsorbates increase the coordination of the surface Pt, thereby relaxing the structure and increasing crystallinity.

Size-dependent structure in metal oxide nanoparticles

Metal oxides have a wide variety of applications including energy production and storage[154,155] human health,[156] and environmental remediation[157] that rely on size-dependent properties.[158] Synthetic control of size and structure has been harder to achieve in the synthesis of metal oxide nanoparticles compared to metallic or metal chalcogenide nanoparticles,[159] and generally, the effects of nanosizing on atomic structure are less clear compared to *e.g.* the simple metallic structures as described above. A wealth of different metal oxide crystal structures exists that are commonly composed of tetrahedrally and octahedrally coordinated cations forming a range of canonical metal oxide structures that include *e.g.* the rutile, perovskite and spinel structures. The common structural units, trends in crystal chemistry and known defect motifs from bulk materials provide a valuable toolbox when characterizing size-dependent structures of metal oxide nanomaterials.

Defects in oxide nanoparticles. An example of a material where the atomic structure changes significantly when nano-sized is molybdenum oxide.[131] MoO_2 normally crystallizes in a distorted rutile structure, however, diffraction data showed indications of a significant structural change on the nanoscale.[160] To gain further insight on the nanoscale structural changes, crystalline nanoparticles (*ca.* 40 nm) and 'nanostructured' (*ca.* 4 nm nanoparticles) MoO_2 were synthesized by simply varying the solvent in a solvothermal synthesis. The crystalline MoO_2 sample was characterized with PXRD and Rietveld refinement, and the data could be fit reasonably well with the known distorted rutile structure. However, the same structural model could not be applied to fit the data from the smaller nanostructured MoO_2 particles, which indicated a fundamental change in the atomic structure. Furthermore, PDFs from the samples showed that the distorted rutile model could only describe the average structure of the crystalline MoO_2 particles. The distorted rutile model failed to fit the PDF peak originating from nearest neighbor Mo–Mo distances in edge-sharing octahedra, where the fit showed that edge-sharing occurred more frequently in the crystalline sample than in the rutile model. The PDF of the crystalline MoO_2 (40 nm) could be modelled by applying a two-phase approach, where the excess edge-sharing in the sample was accounted for by adding a second phase to the fit, a hollandite model. Hollandite contains more edge-sharing [MoO_6] octahedra than rutile and is related to the defect chemistry of rutile.[161] The hollandite model was restricted to the local region of the PDF by applying a spherical envelope which dampened the contribution of the hollandite phase in the high-*r* region, where the rutile model described the data well. The fit showed that the samples contain uncorrelated defects, where excess Mo cations occupy empty octahedrally coordinated sites in the crystal structure leading to more edge-sharing motifs. The defects do not affect the average (distorted rutile) structure in the crystalline 40 nm particles. However, this is not the case for 4 nm nanostructured particles, where the rutile model can neither describe the local nor the average structure. From analyzing the PDF of the 4 nm nanostructured particles, it was found that edge-sharing [MoO_6] motifs were even more prominent than for the crystalline samples. We therefore considered a Magnéli-type structure,[162] previously reported in rutile systems, to find a model that described the nanostructure of MoO_2. An interwoven rutile model was developed, where two rutile structures were superimposed in the same closed packed oxygen lattice by adding a second Mo atom in the interstitial site of the unit cell shifted ($0\ \frac{1}{2}\ 0$) compared to the original Mo atom. This was done using the real-space Rietveld approach. The occupancy of the Mo atoms in the interwoven lattice could be refined to determine the defect density, and from comparison of Fig. 11A and B, it was evident that the interwoven model greatly improved the fit of the nanostructured MoO_2 PDF. HR-TEM shown in Fig. 11C provided strong visual support for the model, where a rutile lattice was overlaid on a bright-field HR-TEM of the nanostructured MoO_2 sample. The image showed that Mo atoms were present in the interstitial sites in the rutile structure. This study showed how defect structures known from bulk materials can completely dominate in nanostructured materials, and change not only the local structure, but also the longer-range atomic order in the nanoparticles.

PDF has been used in a range of other defected oxide systems, where the ability to characterize local structure has allowed a description of the atomic arrangement.[65,163–165] For example, ferrihydrite has been extensively studied with X-ray and neutron PDF over the last decade.[166–168] In a 2007 paper, Michel *et al.* suggested a ferrihydrite structure using X-ray PDF, which resembles a Baker–Figgis δ-Keggin cluster structural motif.[166,168] After some controversy regarding this model, the structure of ferrihydrite was further analyzed by Harrington *et al.* using neutron total scattering with PDF analysis. They found that the single phase model containing a Keggin motif best described the data compared to other 2-phase models proposed in the literature.[167] As an important point, the authors emphasized that the model is merely a representation of the ensemble average structure: When characterizing highly defective nanoscale materials, any simple model will be unlikely

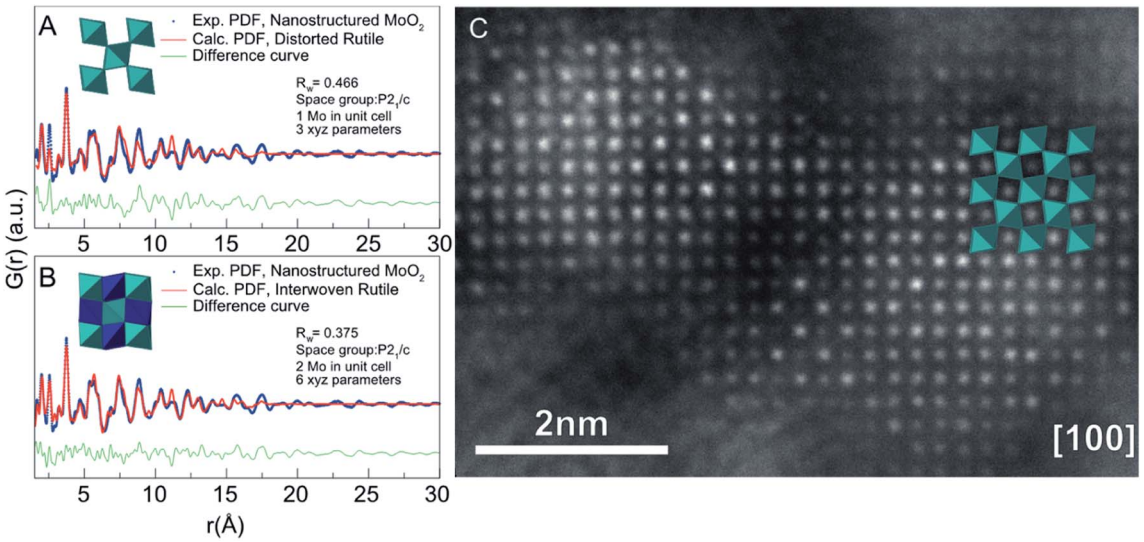

Fig. 11 Fits to PDFs from nanostructured molybdenum oxide using different structural models. (A) Fit of the data with a bulk rutile structure and (B) with an 'interwoven' rutile model. (C) High-resolution annular dark field TEM image obtained from the sample, overlaid with the rutile structure. The image shows intensity in the unoccupied sites in the rutile structure. Reprinted with permission from Lindahl Christiansen *et al.*, *ACS Nano*, 2019, **13**, 8725–8735.[131] Copyright 2019 American Chemical Society.

to fully describe the structures in samples with *e.g.* a distribution of crystallite domain sizes and structures that are difficult to parameterize. A model for such disordered systems should be seen as describing the most important structural motifs and as a starting point for further analysis. In order to better understand ferrihydrite, recent work was done concerning the structure of an aluminum analog to ferrihydrite, akdalaite. The structure of akdalaite was determined by single crystal X-ray diffraction, neutron diffraction and NMR,[169] and it was shown to contain a Keggin cluster motif. The calculated PDF of the akdalaite structure was then compared to the experimental PDF of 6-line ferrihydrite and it was found to describe the major structural features, further suggesting that the structure of ferrihydrite resembles that of Keggin clusters. Very recently, Funnel *et al.* used a nanocomposite RMC methodology for further analysis of X-ray PDFs from ferrihydrite. Here, it was shown that the single phase model from Michel *et al.* gave the best fit to the data without any unphysical structural rearrangements.[170]

Domain structures in disordered oxide structures. PDF has been used to characterize domain structures in many highly disordered or nanostructured oxide materials, giving new information on *e.g.* the structural motifs important for catalytic activity.[171–174] Du *et al.* investigated the structure of a nanostructured cobalt oxide water splitting catalyst.[175] Previous structural studies of the material using X-ray absorption fine structure (XAFS) had revealed a cubane-type motif consisting of edge-sharing CoO_6 octahedra,[176] and the study aimed to complement these results using PDF where the long range atomic correlations are more accessible. Various cobalt oxide models were built with different domain sizes, aspect ratios and lattice structures, and PDFs were calculated from the models using the Debye equation and compared to the experimental PDFs. An appropriate model with 13 Co atoms could be cut directly from a $LiCoO_2$ crystal structure, and the comparison to the experimental PDF is shown in Fig. 12A. The model gives a good description of the experimental PDF, and each peak could be assigned to a particular atomic distance in the model. A misfit is seen between model and data in peaks c and g that originate from the Co–O correlations shown in the insert in Fig. 12A. The misfit could be remedied by a small shift in the atomic position of the terminal oxygens, which shortens some of the distances associated with peaks c and g by 0.2 Å, now labelled c′ and g′. With the small change, an excellent agreement between data and model is obtained with an *R*-value of 0.19 as shown in Fig. 12B. A peak at 1.5 Å was also not described by the model, which is assigned to a P–O distance, and an improved model was made by including phosphate groups in the structure.

Particle faceting and morphology: combination of PDF with other scattering methods. Several other oxide nanomaterials have been studied with PDF. For example, TiO_2 is among the most widely studied oxides due to its applications in *e.g.* photocatalysis,[177,178] and it has also been the subject of several PDF studies.[179–185] One study focused on a combination of scattering techniques for the analysis of TiO_2 (B) nanocrystal morphology and faceting.[186] These particles are prone to aggregation which made unambiguous morphology determinations by TEM difficult. Instead, the morphology was investigated using SAXS, PXRD and PDF, and the combination of all these techniques was demonstrated to be an excellent and necessary way to extract morphological information. Initially, the SAXS data were fit using three particle shapes that were likely based on TEM results and previous studies: spherical, prolate (one expanded axis) and oblate (one contracted axis). All three SAXS fits were of similar quality and the crystallite shape could not be

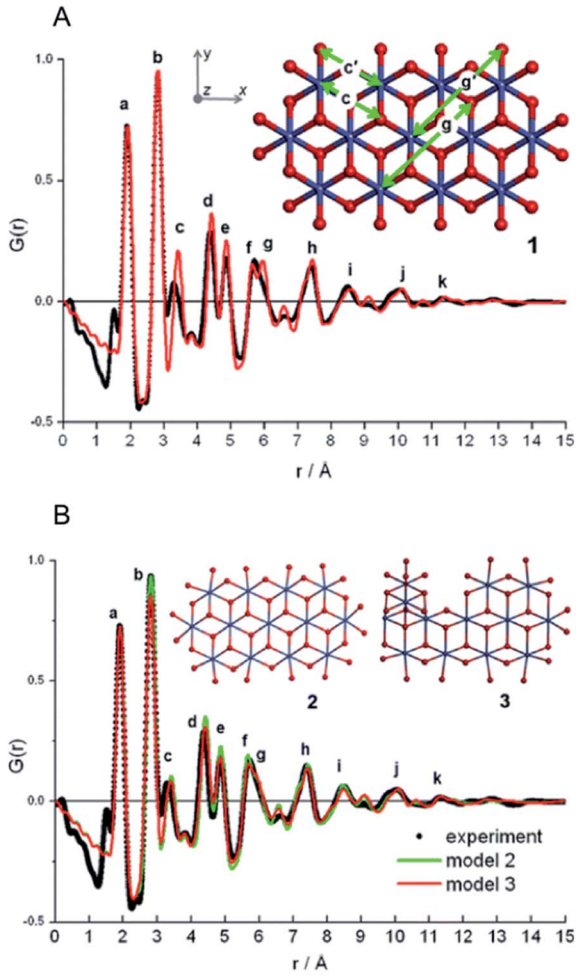

Fig. 12 Fits to PDF from nanostructured cobalt oxide. (A) Fit of the PDF from model 1 (red) to the experimental PDF (black). (B) Fit of the PDF from model 2 (red) and model 3 (green), compared to the experimental PDF in black. R_w is 0.27 for structure 1 and 0.19 for structures 2 and 3. Adapted with permission from Du *et al., J. Am. Chem. Soc.*, 2012, **134**, 11096–11099.[175] Copyright 2012 American Chemical Society.

distinguished from the SAXS data, however the fits yielded approximate particle sizes. As mentioned, a spherical envelope function is often assumed for crystallite size determination in real-space Rietveld refinements. However, such fits yielded poor agreement at high *r*, alluding to a different shape of the particles than spherical. The same conclusion was also drawn from the PXRD patterns. To combine the information from the various techniques, discrete particle models with spherical, prolate and oblate shapes were constructed using the size and aspect ratio determined from PDF and SAXS. Using the Debye equation, these particle models could be tested against the PDF and PXRD data, and the oblate shape with a contraction along the crystallographic *b* axis was shown to best describe the data.

The combination of PDF with other scattering techniques gives many possibilities for structural insight. Farrow *et al.* showed that *complex modelling* of combined SAXS and PDF data allowed a more robust characterization of CdS nanoparticle morphology[187] as can be applied in Diffpy-CMI.[62] Many more studies of this kind is likely to be seen in the literature in the future.

Metal sorption on oxide nanoparticle surfaces: d-PDF studies. As described above, the use of d-PDF gives many options for studying supported materials and surface interactions. d-PDF studies have also been widely used in studies of oxide materials, *e.g.* for analysis of catalytically active sites,[188] and for studies of heavy metal sorption in ferrihydrite.[38,107,189,190] For example, d-PDF was used in order to characterize the binding geometry of AsO_4 on ferrihydrite.[38] The d-PDFs showed clear peaks arising from As–O and As–Fe correlations, which were used to show that AsO_4 binds bidentate to the ferrihydrite structure. In contrast to this, d-PDF showed that SbO_6 binds by both a bidentate mononuclear structure (single edge sharing) and a bidentate binuclear structure, although the binding geometry of SbO_6 octahedra was anticipated to be the same as AsO_4 tetrahedra.[191] The increased sorption capacity of Sb on ferrihydrite compared to As was determined to be due to the similarity of the SbO_6 to the FeO_6 octahedra in terms of size and shape, allowing SbO_6 to incorporate into the structure more easily.

PDF analysis of disordered layered oxide materials. The high flexibility and tunability in structure and chemical composition of many layered metal oxide materials allow for extensive intercalation of ions and molecules, opening for a wealth of applications in *e.g.* battery electrodes,[192,193] catalysis,[194] environmental remediation,[195] and in a range of other technologies relying on ion exchange and storage.[196] Many layered oxides show a high degree of inter- and intralayer disorder, and several structures have been extensively studied with PDF.[77,197–202]

The complex challenges involved in structural characterization of disordered layered oxides are addressed in an extensive study of the structure of δ-MnO_2 by Liu *et al.*[199] Layered metal oxides are often small nanoparticles, contain turbostatic stacking faults and exhibit in-plane cation disorder. Liu *et al.* address all three aspects of the structural complexity in a study of Cu-rich δ-MnO_2 (ref. 199) using X-ray total scattering and PDF, supported by a range of techniques, including EXAFS and neutron PDF. The local structure in the planes of the layered oxide was first determined by fitting the 0.7–8 Å range of the PDF. Cu^{2+} ions were localized in the structure by comparing a model where Cu^{2+} was placed in the Mn^{4+} sites of the layer, or a model where the Cu^{2+} was placed between the layers of the structure. It was found that the Cu^{2+} ions sit in interplanar sites above or below a vacant Mn^{4+} site. Next, the in-plane vacancy ordering was determined by comparing fits of different cation vacancy ordering models applied only to the local range of the PDF, where only intraplanar distances are represented. A chalcophanite structure model with 7.2% Mn vacancy was found to most suitably describe the in-plane atomic arrangement, with a good agreement factor of 8.2%. The local structure description is further extended by locating the interlayer H_2O using neutron PDF, which is possible due to the greater sensitivity to H (or D) when using neutrons instead of X-rays in a scattering experiment. Finally, using the local atomic structure model already developed, a model for the stacking disorder was built by

creating a supercell containing 7 layers with the refined local layer structure. Each layer was assigned three vectors (t_a, t_b, t_c), one for each crystallographic axis, that allowed the atomic structure in the layer to remain unchanged, while the layers can move with respect to each other. Furthermore, a numerical particle shape correction was applied that replaced the usual spherical envelope function and improves the long-range fit of the PDF for the non-spherical particles.[63] The final stacking fault model provided a good description of scattering data in both Q and r for both X-rays and neutrons. The refined values of the in-plane layer vectors (t_a and t_b), appeared largely random, while the vectors in the stacking direction remained unchanged, which was interpreted as the stacking faults being associated with rotational disorder. This study showcases a highly inventive way of extending the local structural information available in the PDF to describe the full nanostructure of a complex sample.

In situ and *operando* experiments: changes in nanoparticle structure

Having established the strength of PDF analysis for nanomaterial characterization, we here only briefly mention the importance of *in situ* and *operando* PDF analysis in nanomaterials chemistry, as these fields have been reviewed in the past.[32,33,37] *In situ* X-ray or neutron powder diffraction, where diffraction patterns are continuously collected during a chemical reaction, has a long and successful history dating back to the 1990s, and excels when investigating bulk crystalline phase transitions and crystallite growth kinetics.[203–206] *In situ* PDF studies, on the other hand, allow for identification and characterization of disordered or amorphous intermediate structures and species in solution, which are important in nanomaterials. For example, in studies of nanomaterial synthesis, *in situ* PDF analysis gives the possibility for studying the atomic structure of the species present before, during and after crystallization of nanoparticles,[183,207–219] which is essential for gaining a deeper understanding of material nucleation processes, where atomic scale mechanistic information generally is scarce. Knowledge of the relation between chemical synthesis and the resulting atomic structure of the material is crucial in the advancement of nanoscience.[220] In studies of battery materials, *operando* experiments allow following the changes in electrode structure during operation, and the use of PDF has revealed complex reactions, where disordered nanomaterials play a large role in the cycling processes.[221–229]

Summary and future perspectives

We have reviewed a number of studies where atomic structure on the nanoscale has been characterized using PDF. Structural studies of metals, chalcogenides and oxides were described, covering a range of different approaches to PDF analysis, including model-free analysis, real-space Rietveld refinement, d-PDF analysis, and modelling using discrete structures with the Debye scattering equation. The PDF technique is growing in importance, and many other emerging nanomaterials such as perovskites,[36,230–232] upconverting nanoparticles,[34,233] sulfides,[234–236] nitrides and carbides[237–242] are now being investigated with PDF. The diversity of the studies demonstrates an important point: there is no *one-fits-all* approach to PDF modelling of the structure of nanoparticles, and the method to be used is dependent on the problem that is under investigation, and what information is sought. This means that constructing a good structural model for a nanostructure from PDF analysis requires a great deal of creativity, structural understanding and chemical intuition, however the simplicity and intuitive nature of the PDF can be helpful in achieving a good starting point.

While PDF analysis can be extremely useful for analysis of atomic structure, one always has to be aware of its limitations: the PDF will not always contain enough information to determine a unique model for atomic structure. This problem is only amplified by the disordered and polydisperse nature of most nanomaterials, and careful consideration should be given to the uniqueness and validity of any model constructed. It is paramount that PDF models are supported by structural information from other techniques. One perspective on tackling this issue is the *complex modelling* approach, where one structural model is refined against multiple datasets from different techniques.[62,73,243] This makes the models and refined parameters more reliable, as they have been constrained by structural information obtained from techniques with different strengths and weaknesses, such as when combining PDF or total scattering with SAXS[95,187,244] or EXAFS data.[74,245]

The interest and development of advanced computational techniques such as database mining and machine learning are very likely to impact PDF analysis as well as many other data-heavy fields in the coming years.[246] For example, machine learning methods have already been applied to PDF in regards to component analysis[123,247–250] and in identifying symmetry and extracting distance lists.[251,252] This development is likely to aid in maximizing the information that can be extracted from the PDF of complicated nanostructures. Automated modelling, where large numbers of structures (mined from databases or algorithmically generated) are fitted to experimental PDFs, can improve the structural characterization workflow and the discovery of new and improved models.[127,128,253] However, presently, the more advanced tools for modelling and constructing new nanostructures are somewhat un-accessible to the broad scientific community, and the development of user-friendly software and tools for more advanced analysis should be a high priority within the PDF community.

While these new advanced developments are hugely important, we stress that significant information can be extracted from PDF analysis using relatively simple methods, such as real-space Rietveld refinement or model-free analysis of individual peaks, and PDF will prove useful in the toolbox of any scientist wishing to characterize nanostructures. With this review, we hope to have provided an entry into PDF analysis, and we invite everyone to join the journey down the yellow brick road towards better understanding of structure on the nanoscale.

Conflicts of interest

There are no conflicts to declare.

Acknowledgements

We are grateful to the Villum Foundation for financial support through a Villum Young Investigator grant. KMØJ acknowledges funding from the Danish Research Council under the Sapere Aude Research Talent Program. This work is part of a project that has received funding from the European Research Council (ERC) under the European Union's Horizon 2020 research and innovation programme, (Grant agreement no. 804066). This project has received funding from the European Union's Horizon 2020 research and innovation programme under the Marie Sklodowska-Curie grant agreement no. 841903.

References

1 D. Schwarzenbach, *Acta Crystallogr., Sect. A: Found. Crystallogr.*, 2012, **68**, 57–67.
2 *Nat. Mater.*, 2014, **13**, 757.
3 M. Eckert, *Acta Crystallogr., Sect. A: Found. Crystallogr.*, 2012, **68**, 30–39.
4 W. L. Bragg, *Proc. R. Soc. London, Ser. A*, 1913, **89**, 248–277.
5 W. Friedrich, P. Knipping and M. Laue, *Ann. Phys.*, 1913, **346**, 971–988.
6 H. M. Rietveld, *J. Appl. Crystallogr.*, 1969, **2**, 65–71.
7 A. K. Cheetham and A. L. Goodwin, *Nat. Mater.*, 2014, **13**, 760–762.
8 M. Etter and R. E. Dinnebier, *Z. Anorg. Allg. Chem.*, 2014, **640**, 3015–3028.
9 J. Wood, *Mater. Today*, 2008, **11**, 40–45.
10 W. J. Stark, P. R. Stoessel, W. Wohlleben and A. Hafner, *Chem. Soc. Rev.*, 2015, **44**, 5793–5805.
11 M. V. Kovalenko, L. Manna, A. Cabot, Z. Hens, D. V. Talapin, C. R. Kagan, V. I. Klimov, A. L. Rogach, P. Reiss, D. J. Milliron, P. Guyot-Sionnnest, G. Konstantatos, W. J. Parak, T. Hyeon, B. A. Korgel, C. B. Murray and W. Heiss, *ACS Nano*, 2015, **9**, 1012–1057.
12 E. Roduner, *Chem. Soc. Rev.*, 2006, **35**, 583–592.
13 V. H. Grassian, *J. Phys. Chem. C*, 2008, **112**, 18303–18313.
14 M. Auffan, J. Rose, J.-Y. Bottero, G. V. Lowry, J.-P. Jolivet and M. R. Wiesner, *Nat. Nanotechnol.*, 2009, **4**, 634–641.
15 C. L. Cleveland, U. Landman, T. G. Schaaff, M. N. Shafigullin, P. W. Stephens and R. L. Whetten, *Phys. Rev. Lett.*, 1997, **79**, 1873–1876.
16 N. Goswami, Q. Yao, T. Chen and J. Xie, *Coord. Chem. Rev.*, 2016, **329**, 1–15.
17 H. Qian, M. Zhu, Z. Wu and R. Jin, *Acc. Chem. Res.*, 2012, **45**, 1470–1479.
18 E. C. Tyo and S. Vajda, *Nat. Nanotechnol.*, 2015, **10**, 577–588.
19 S. J. L. Billinge and I. Levin, *Science*, 2007, **316**, 561–565.
20 B. Ingham, *Crystallogr. Rev.*, 2015, **21**, 229–303.
21 D. Balzar, N. Audebrand, M. R. Daymond, A. Fitch, A. Hewat, J. I. Langford, A. Le Bail, D. Louer, O. Masson, C. N. McCowan, N. C. Popa, P. W. Stephens and B. H. Toby, *J. Appl. Crystallogr.*, 2004, **37**, 911–924.
22 T. Egami and S. J. Billinge, *Underneath the Bragg peaks: Structural analysis of complex materials*, Elsevier, Amsterdam, 2nd edn, 2012.
23 E. K. Richman and J. E. Hutchison, *ACS Nano*, 2009, **3**, 2441–2446.
24 A. Kuzmin and J. Chaboy, *IUCrJ*, 2014, **1**, 571–589.
25 J. Miao, P. Ercius and S. J. L. Billinge, *Science*, 2016, **353**, aaf2157.
26 Y. Yang, C.-C. Chen, M. C. Scott, C. Ophus, R. Xu, A. Pryor, L. Wu, F. Sun, W. Theis, J. Zhou, M. Eisenbach, P. R. C. Kent, R. F. Sabirianov, H. Zeng, P. Ercius and J. Miao, *Nature*, 2017, **542**, 75–79.
27 D. A. Muller, *Nat. Mater.*, 2009, **8**, 263–270.
28 S. J. L. Billinge and M. G. Kanatzidis, *Chem. Commun.*, 2004, **7**, 749–760.
29 K. Page, T. Proffen and R. Neder, in *Modern Diffraction Methods*, ed. E. J. Mittemeijer and U. Welzel, 2013, pp. 61–86, DOI: 10.1002/9783527649884.ch3.
30 T. Egami, H. D. Rosenfeld, B. H. Toby and A. Bhalla, *Ferroelectrics*, 1991, **120**, 11–21.
31 S. J. L. Billinge, *Philos. Trans. R. Soc. London, Ser. A*, 2019, **377**, 20180413.
32 E. D. Bøjesen and B. B. Iversen, *CrystEngComm*, 2016, **18**, 8332–8353.
33 K. W. Chapman, *MRS Bull.*, 2016, **41**, 231–240.
34 S. S. Perera, D. K. Amarasinghe, K. T. Dissanayake and F. A. Rabuffetti, *Chem. Mater.*, 2017, **29**, 6289–6297.
35 R. B. Soriano, I. U. Arachchige, C. D. Malliakas, J. Wu and M. G. Kanatzidis, *J. Am. Chem. Soc.*, 2013, **135**, 768–774.
36 F. A. Rabuffetti and R. L. Brutchey, *ACS Nano*, 2013, **7**, 11435–11444.
37 K. M. Ø. Jensen, C. Tyrsted, M. Bremholm and B. B. Iversen, *ChemSusChem*, 2014, **7**, 1594–1611.
38 R. Harrington, D. B. Hausner, N. Bhandari, D. R. Strongin, K. W. Chapman, P. J. Chupas, D. S. Middlemiss, C. P. Grey and J. B. Parise, *Inorg. Chem.*, 2010, **49**, 325–330.
39 X. Wang, J. D. Kubicki, J.-F. Boily, G. A. Waychunas, Y. Hu, X. Feng and M. Zhu, *ACS Earth Space Chem.*, 2018, **2**, 125–134.
40 R. Harrington, R. B. Neder and J. B. Parise, *Chem. Geol.*, 2012, **329**, 3–9.
41 S. Thakral, M. W. Terban, N. K. Thakral and R. Suryanarayanan, *Adv. Drug Delivery Rev.*, 2016, **100**, 183–193.
42 S. J. L. Billinge, *Nanomedicine*, 2015, **10**, 2473–2475.
43 M. W. Terban, M. Johnson, M. Di Michiel and S. J. L. Billinge, *Nanoscale*, 2015, **7**, 5480–5487.
44 P. J. Chupas, X. Y. Qiu, J. C. Hanson, P. L. Lee, C. P. Grey and S. J. L. Billinge, *J. Appl. Crystallogr.*, 2003, **36**, 1342–1347.
45 C. L. Farrow, P. Juhas, J. W. Liu, D. Bryndin, E. S. Bozin, J. Bloch, T. Proffen and S. J. L. Billinge, *J. Phys.: Condens. Matter*, 2007, **19**, 335219.
46 P. Juhas, T. Davis, C. L. Farrow and S. J. L. Billinge, *J. Appl. Crystallogr.*, 2013, **46**, 560–566.
47 A. A. Coelho, P. A. Chater and A. Kern, *J. Appl. Crystallogr.*, 2015, **48**, 869–875.

48 A. K. Soper, *GudrunN and GudrunX: programs for correcting raw neutron and X-ray diffraction data to differential scattering cross section*, Science & Technology Facilities Council Swindon, UK, 2011.
49 B. H. Toby and R. B. Von Dreele, *J. Appl. Crystallogr.*, 2013, **46**, 544–549.
50 S. J. L. Billinge, *Z. Kristallogr.*, 2004, **219**, 117–121.
51 C. A. Young and A. L. Goodwin, *J. Mater. Chem.*, 2011, **21**, 6464–6476.
52 T. Proffen, K. L. Page, S. E. McLain, B. Clausen, T. W. Darling, J. A. TenCate, S. Y. Lee and E. Ustundag, *Z. Kristallogr.*, 2005, **220**, 1002–1008.
53 A. S. Masadeh, *J. Exp. Nanosci.*, 2016, **11**, 951–974.
54 P. Bordet, *C. R. Phys.*, 2018, **19**, 561–574.
55 T. Proffen, S. J. L. Billinge, T. Egami and D. Louca, *Z. Kristallogr.*, 2003, **218**, 132–143.
56 S. J. L. Billinge and R. E. Dinnebier, *Powder Diffraction: Theory and Practice*, RSC Publishing, Cambridge, 2008.
57 P. F. Peterson, M. Gutmann, T. Proffen and S. J. L. Billinge, *J. Appl. Crystallogr.*, 2000, **33**, 1192.
58 P. Juhas, J. N. Louwen, L. van Eijck, E. T. C. Vogt and S. J. L. Billinge, *J. Appl. Crystallogr.*, 2018, **51**, 1492–1497.
59 S. L. J. Thomae, N. Prinz, T. Hartmann, M. Teck, S. Correll and M. Zobel, *Rev. Sci. Instrum.*, 2019, **90**, 043905.
60 A. M. M. Abeykoon, C. D. Malliakas, P. Juhás, E. S. Bozin, M. G. Kanatzidis and S. J. L. Billinge, *Z. Kristallogr. - Cryst. Mater.*, 2012, **227**, 248.
61 D. Keen, *J. Appl. Crystallogr.*, 2001, **34**, 172–177.
62 P. Juhas, C. L. Farrow, X. Yang, K. R. Knox and S. J. L. Billinge, *Acta Crystallogr., Sect. A: Found. Adv.*, 2015, **71**, 562–568.
63 T.-M. Usher, D. Olds, J. Liu and K. Page, *Acta Crystallogr., Sect. A: Found. Adv.*, 2018, **74**, 322–331.
64 L. Gamez-Mendoza, M. W. Terban, S. J. L. Billinge and M. Martinez-Inesta, *J. Appl. Crystallogr.*, 2017, **50**, 741–748.
65 G. Paglia, E. S. Bozin and S. J. L. Billinge, *Chem. Mater.*, 2006, **18**, 3242–3248.
66 P. Debye and P. Scherrer, *Phys. Z.*, 1916, **17**, 277–283.
67 B. D. Hall and R. Monot, *Comput. Phys.*, 1991, **5**, 414–417.
68 T. Proffen and R. B. Neder, *J. Appl. Crystallogr.*, 1997, **30**, 171–175.
69 F. Bertolotti, D. Moscheni, A. Guagliardi and N. Masciocchi, *Eur. J. Inorg. Chem.*, 2018, **2018**, 3789–3803.
70 A. Cervellino, R. Frison, F. Bertolotti and A. Guagliardi, *J. Appl. Crystallogr.*, 2015, **48**, 1600–5767.
71 M. G. Tucker, D. A. Keen, M. T. Dove, A. L. Goodwin and Q. Hui, *J. Phys.: Condens. Matter*, 2007, **19**, 335218.
72 M. T. Dove, M. G. Tucker and D. A. Keen, *Eur. J. Mineral.*, 2002, **14**, 331–348.
73 M. J. Cliffe, M. T. Dove, D. Drabold and A. L. Goodwin, *Phys. Rev. Lett.*, 2010, **104**, 125501.
74 M. Harada, R. Ikegami, L. S. R. Kumara, S. Kohara and O. Sakata, *RSC Adv.*, 2019, **9**, 29511–29521.
75 V. Petkov, C. M. Hessel, J. Ovtchinnikoff, A. Guillaussier, B. A. Korgel, X. Liu and C. Giordano, *Chem. Mater.*, 2013, **25**, 2365–2371.
76 J. A. Vargas, V. Petkov, E. S. A. Nouh, R. K. Ramamoorthy, L.-M. Lacroix, R. Poteau, G. Viau, P. Lecante and R. Arenal, *ACS Nano*, 2018, **12**, 9521–9531.
77 V. Petkov, S. J. L. Billinge, P. Larson, S. D. Mahanti, T. Vogt, K. K. Rangan and M. G. Kanatzidis, *Phys. Rev. B: Condens. Matter Mater. Phys.*, 2002, **65**, 092105.
78 V. Petkov, S. J. L. Billinge, J. Heising and M. G. Kanatzidis, *J. Am. Chem. Soc.*, 2000, **122**, 11571–11576.
79 R. B. Neder and V. I. Korsunskiy, *J. Phys.: Condens. Matter*, 2005, **17**, S125–S134.
80 V. I. Korsounski, R. B. Neder, K. Hradil, C. Barglik-Chory, G. Muller and J. Neuefeind, *J. Appl. Crystallogr.*, 2003, **36**, 1389–1396.
81 D. C. Gary, M. W. Terban, S. J. L. Billinge and B. M. Cossairt, *Chem. Mater.*, 2015, **27**, 1432–1441.
82 A. Demortière, D. N. Leonard, V. Petkov, K. Chapman, S. Chattopadhyay, C. She, D. A. Cullen, T. Shibata, M. Pelton and E. V. Shevchenko, *J. Phys. Chem. Lett.*, 2018, **9**, 1900–1906.
83 J. Owen and L. Brus, *J. Am. Chem. Soc.*, 2017, **139**, 10939–10943.
84 A. Eychmüller, *J. Phys. Chem. B*, 2000, **104**, 6514–6528.
85 S. M. Harrell, J. R. McBride and S. J. Rosenthal, *Chem. Mater.*, 2013, **25**, 1199–1210.
86 A. S. Masadeh, E. S. Bozin, C. L. Farrow, G. Paglia, P. Juhas, S. J. L. Billinge, A. Karkamkar and M. G. Kanatzidis, *Phys. Rev. B*, 2007, **76**, 115413.
87 C. B. Murray, D. J. Norris and M. G. Bawendi, *J. Am. Chem. Soc.*, 1993, **115**, 8706–8715.
88 M. G. Bawendi, A. R. Kortan, M. L. Steigerwald and L. E. Brus, *J. Chem. Phys.*, 1989, **91**, 7282–7290.
89 X. Yang, A. S. Masadeh, J. R. McBride, E. S. Božin, S. J. Rosenthal and S. J. L. Billinge, *Phys. Chem. Chem. Phys.*, 2013, **15**, 8480–8486.
90 W. Vogel, P. H. Borse, N. Deshmukh and S. K. Kulkarni, *Langmuir*, 2000, **16**, 2032–2037.
91 P.-J. Wu, Y. P. Stetsko, K.-D. Tsuei, R. Dronyak and K. S. Liang, *Appl. Phys. Lett.*, 2007, **90**, 161911.
92 C. Kumpf, R. B. Neder, F. Niederdraenk, P. Luczak, A. Stahl, M. Scheuermann, S. Joshi, S. K. Kulkarni, C. Barglik-Chory, C. Heske and E. Umbach, *J. Chem. Phys.*, 2005, **123**, 224707.
93 F. Bertolotti, A. H. Proppe, D. N. Dirin, M. Liu, O. Voznyy, A. Cervellino, S. J. L. Billinge, M. V. Kovalenko, E. H. Sargent, N. Masciocchi and A. Guagliardi, *Chem. Sq.*, 2018, **2**, 1.
94 R. B. Neder, V. I. Korsunskiy, C. Chory, G. Müller, A. Hofmann, S. Dembski, C. Graf and E. Rühl, *Phys. Status Solidi C*, 2007, **4**, 3221–3233.
95 D. Moscheni, F. Bertolotti, L. Piveteau, L. Protesescu, D. N. Dirin, M. V. Kovalenko, A. Cervellino, J. S. Pedersen, N. Masciocchi and A. Guagliardi, *ACS Nano*, 2018, **12**, 12558–12570.
96 F. Niederdraenk, K. Seufert, A. Stahl, R. S. Bhalerao-Panajkar, S. Marathe, S. K. Kulkarni, R. B. Neder and C. Kumpf, *Phys. Chem. Chem. Phys.*, 2011, **13**, 498–505.
97 F. Niederdraenk, K. Seufert, P. Luczak, S. K. Kulkarni, C. Chory, R. B. Neder and C. Kumpf, *Phys. Status Soldi C*, 2007, **4**, 3234–3243.

98 E. S. Bozin, C. D. Malliakas, P. Souvatzis, T. Proffen, N. A. Spaldin, M. G. Kanatzidis and S. J. L. Billinge, *Science*, 2010, **330**, 1660–1663.
99 F. Bertolotti, D. N. Dirin, M. Ibáñez, F. Krumeich, A. Cervellino, R. Frison, O. Voznyy, E. H. Sargent, M. V. Kovalenko, A. Guagliardi and N. Masciocchi, *Nat. Mater.*, 2016, **15**, 987–994.
100 K. Yu, *Adv. Mater.*, 2012, **24**, 1123–1132.
101 A. N. Beecher, X. Yang, J. H. Palmer, A. L. LaGrassa, P. Juhas, S. J. L. Billinge and J. S. Owen, *J. Am. Chem. Soc.*, 2014, **136**, 10645–10653.
102 J. L. Stein, M. I. Steimle, M. W. Terban, A. Petrone, S. J. L. Billinge, X. Li and B. M. Cossairt, *Chem. Mater.*, 2017, **29**, 7984–7992.
103 L. Tan, A. J. Misquitta, A. Sapelkin, L. Fang, R. M. Wilson, D. S. Keeble, B. Zhang, T. Zhu, F. S. Riehle, S. Han, K. Yu and M. T. Dove, *Nanoscale*, 2019, **11**, 21900–21908.
104 B. Gilbert, F. Huang, H. Zhang, G. A. Waychunas and J. F. Banfield, *Science*, 2004, **305**, 651–654.
105 G. R. Schleder, G. M. Azevedo, I. C. Nogueira, Q. H. F. Rebelo, J. Bettini, A. Fazzio and E. R. Leite, *J. Phys. Chem. Lett.*, 2019, **10**, 1471–1476.
106 B. M. Cossairt, P. Juhas, S. J. L. Billinge and J. S. Owen, *J. Phys. Chem. Lett.*, 2011, **2**, 3075–3080.
107 H.-W. Wang, D. J. Wesolowski, T. E. Proffen, L. Vlcek, W. Wang, L. F. Allard, A. I. Kolesnikov, M. Feygenson, L. M. Anovitz and R. L. Paul, *J. Am. Chem. Soc.*, 2013, **135**, 6885–6895.
108 H. Zhang, B. Gilbert, F. Huang and J. F. Banfield, *Nature*, 2003, **424**, 1025–1029.
109 R. Sardar, A. M. Funston, P. Mulvaney and R. W. Murray, *Langmuir*, 2009, **25**, 13840–13851.
110 C. Xie, Z. Niu, D. Kim, M. Li and P. Yang, *Chem. Rev.*, 2020, **120**, 1184–1249.
111 T. Ishida, T. Murayama, A. Taketoshi and M. Haruta, *Chem. Rev.*, 2020, **120**, 464–525.
112 L. D. Marks and A. Howie, *Nature*, 1979, **282**, 196–198.
113 L. D. Marks, *Rep. Prog. Phys.*, 1994, **57**, 603–649.
114 A. Mackay, *Acta Crystallogr.*, 1962, **15**, 916–918.
115 S. Hajiw, B. Pansu and J.-F. Sadoc, *ACS Nano*, 2015, **9**, 8116–8121.
116 F. C. Frank and J. S. Kasper, *Acta Crystallogr.*, 1959, **12**, 483–499.
117 H. Nakotte, C. Silkwood, K. Page, H. W. Wang, D. Olds, B. Kiefer, S. Manna, D. Karpov, E. Fohtung and E. E. Fullerton, *Phys. Scr.*, 2017, **92**, 114002.
118 S. Ino, *J. Phys. Soc. Jpn.*, 1969, **27**, 941–953.
119 L. D. Marks, *J. Cryst. Growth*, 1983, **61**, 556–566.
120 K. Page, T. Proffen, H. Terrones, M. Terrones, L. Lee, Y. Yang, S. Stemmer, R. Seshadri and A. K. Cheetham, *Chem. Phys. Lett.*, 2004, **393**, 385–388.
121 V. Petkov, Y. Peng, G. Williams, B. Huang, D. Tomalia and Y. Ren, *Phys. Rev. B: Condens. Matter Mater. Phys.*, 2005, **72**, 195402.
122 A. Hjorth Larsen, J. Jørgen Mortensen, J. Blomqvist, I. E. Castelli, R. Christensen, M. Dułak, J. Friis, M. N. Groves, B. Hammer, C. Hargus, E. D. Hermes, P. C. Jennings, P. Bjerre Jensen, J. Kermode, J. R. Kitchin, E. Leonhard Kolsbjerg, J. Kubal, K. Kaasbjerg, S. Lysgaard, J. Bergmann Maronsson, T. Maxson, T. Olsen, L. Pastewka, A. Peterson, C. Rostgaard, J. Schiøtz, O. Schütt, M. Strange, K. S. Thygesen, T. Vegge, L. Vilhelmsen, M. Walter, Z. Zeng and K. W. Jacobsen, *J. Phys.: Condens. Matter*, 2017, **29**, 273002.
123 W. Li, O. J. Borkiewicz, M. Saubanère, M.-L. Doublet, D. Flahaut, P. J. Chupas, K. W. Chapman and D. Dambournet, *J. Phys. Chem. C*, 2018, **122**, 23861–23866.
124 W. A. Sławiński, E. Zacharaki, H. Fjellvåg and A. O. Sjåstad, *Cryst. Growth Des.*, 2018, **18**, 2316–2325.
125 J. A. Oberteuffer and J. A. Ibers, *Acta Crystallogr., Sect. B: Struct. Crystallogr. Cryst. Chem.*, 1970, **26**, 1499–1504.
126 S. Banerjee, C.-H. Liu, J. D. Lee, A. Kovyakh, V. Grasmik, O. Prymak, C. Koenigsmann, H. Liu, L. Wang, A. M. M. Abeykoon, S. S. Wong, M. Epple, C. B. Murray and S. J. L. Billinge, *J. Phys. Chem. C*, 2018, **122**, 29498–29506.
127 S. Banerjee, C.-H. Liu, K. M. Ø. Jensen, P. Juhas, J. D. Lee, M. Tofanelli, C. J. Ackerson, C. B. Murray and S. J. L. Billinge, *Acta Crystallogr., Sect. A: Found. Adv.*, 2020, **76**, 24–31.
128 T. Lindahl Christiansen, E. T. S. Kjær, A. Kovyakh, M. L. Röderen, M. Høj, T. Vosch and K. M. Ø. Jensen, *J. Appl. Crystallogr.*, 2020, **53**, 148–158.
129 V. V. T. Doan-Nguyen, S. A. J. Kimber, D. Pontoni, D. Reifsnyder Hickey, B. T. Diroll, X. Yang, M. Miglierini, C. B. Murray and S. J. L. Billinge, *ACS Nano*, 2014, **8**, 6163–6170.
130 L. B. Skinner, C. J. Benmore, J. K. R. Weber, M. A. Williamson, A. Tamalonis, A. Hebden, T. Wiencek, O. L. G. Alderman, M. Guthrie, L. Leibowitz and J. B. Parise, *Science*, 2014, **346**, 984–987.
131 T. Lindahl Christiansen, E. D. Bøjesen, M. Juelsholt, J. Etheridge and K. M. Ø. Jensen, *ACS Nano*, 2019, **13**, 8725–8735.
132 C. J. Benmore, *ISRN Mater. Sci.*, 2012, **2012**, 852905.
133 H. E. Fischer, A. C. Barnes and P. S. Salmon, *Rep. Prog. Phys.*, 2005, **69**, 233–299.
134 R. Jin, C. Zeng, M. Zhou and Y. Chen, *Chem. Rev.*, 2016, **116**, 10346–10413.
135 R. Jin, *Nanoscale*, 2015, **7**, 1549–1565.
136 S. Tian, Y.-Z. Li, M.-B. Li, J. Yuan, J. Yang, Z. Wu and R. Jin, *Nat. Commun.*, 2015, **6**, 8667.
137 S. F. Li, X. J. Zhao, X. S. Xu, Y. F. Gao and Z. Zhang, *Phys. Rev. Lett.*, 2013, **111**, 115501.
138 C. Kumara, X. Zuo, D. A. Cullen and A. Dass, *ACS Nano*, 2014, **8**, 6431–6439.
139 C. Kumara, X. Zuo, J. Ilavsky, K. W. Chapman, D. A. Cullen and A. Dass, *J. Am. Chem. Soc.*, 2014, **136**, 7410–7417.
140 K. M. Ø. Jensen, P. Juhas, M. A. Tofanelli, C. L. Heinecke, G. Vaughan, C. J. Ackerson and S. J. L. Billinge, *Nat. Commun.*, 2016, **7**, 11859.
141 D. Bahena, N. Bhattarai, U. Santiago, A. Tlahuice, A. Ponce, S. B. H. Bach, B. Yoon, R. L. Whetten, U. Landman and M. Jose-Yacaman, *J. Phys. Chem. Lett.*, 2013, **4**, 975–981.

142 S. J. Tauster, S. C. Fung, R. T. K. Baker and J. A. Horsley, *Science*, 1981, **211**, 1121.
143 R. J. White, R. Luque, V. L. Budarin, J. H. Clark and D. J. Macquarrie, *Chem. Soc. Rev.*, 2009, **38**, 481–494.
144 A. T. Bell, *Science*, 2003, **299**, 1688–1691.
145 K. W. Chapman, P. J. Chupas and C. J. Kepert, *J. Am. Chem. Soc.*, 2005, **127**, 11232–11233.
146 K. W. Chapman, P. J. Chupas, E. R. Maxey and J. W. Richardson, *Chem. Commun.*, 2006, **38**, 4013–4015.
147 P. J. Chupas, K. W. Chapman, H. Chen and C. P. Grey, *Catal. Today*, 2009, **145**, 213–219.
148 M. A. Newton, K. W. Chapman, D. Thompsett and P. J. Chupas, *J. Am. Chem. Soc.*, 2012, **134**, 5036–5039.
149 P. J. Chupas, K. W. Chapman, G. Jennings, P. L. Lee and C. P. Grey, *J. Am. Chem. Soc.*, 2007, **129**, 13822–13824.
150 V. Petkov, Y. Maswadeh, A. Lu, S. Shan, H. Kareem, Y. Zhao, J. Luo, C.-J. Zhong, K. Beyer and K. Chapman, *ACS Appl. Mater. Interfaces*, 2018, **10**, 10870–10881.
151 Y. Lei, H. Zhao, R. D. Rivas, S. Lee, B. Liu, J. Lu, E. Stach, R. E. Winans, K. W. Chapman, J. P. Greeley, J. T. Miller, P. J. Chupas and J. W. Elam, *J. Am. Chem. Soc.*, 2014, **136**, 9320–9326.
152 C. Y. Shi, E. L. Redmond, A. Mazaheripour, P. Juhas, T. F. Fuller and S. J. L. Billinge, *J. Phys. Chem. C*, 2013, **117**, 7226–7230.
153 J. Quinson, L. Kacenauskaite, T. Lindahl Christiansen, T. Vosch, M. Arenz and K. M. Ø. Jensen, *ACS Omega*, 2018, **3**, 10351–10356.
154 Y. Sun, N. Liu and Y. Cui, *Nat. Energy*, 2016, **1**, 16071.
155 X. Chen, C. Li, M. Grätzel, R. Kostecki and S. S. Mao, *Chem. Soc. Rev.*, 2012, **41**, 7909–7937.
156 B. R. Smith and S. S. Gambhir, *Chem. Rev.*, 2017, **117**, 901–986.
157 M. A. Shannon, P. W. Bohn, M. Elimelech, J. G. Georgiadis, B. J. Mariñas and A. M. Mayes, *Nature*, 2008, **452**, 301–310.
158 D. Koziej, A. Lauria and M. Niederberger, *Adv. Mater.*, 2014, **26**, 235–257.
159 S. R. Cooper, L. K. Plummer, A. G. Cosby, P. Lenox, A. Jander, P. Dhagat and J. E. Hutchison, *Chem. Mater.*, 2018, **30**, 6053–6062.
160 D. Koziej, M. D. Rossell, B. Ludi, A. Hintennach, P. Novák, J.-D. Grunwaldt and M. Niederberger, *Small*, 2011, **7**, 377–387.
161 Y. Chabre and J. Pannetier, *Prog. Solid State Chem.*, 1995, **23**, 1–130.
162 L. Kihlborg, in *Nonstoichiometric Compounds*, 1963, vol. 39, ch. 3, pp. 37–45.
163 A. L. Tiano, G. C. Papaefthymiou, C. S. Lewis, J. Han, C. Zhang, Q. Li, C. Y. Shi, A. M. M. Abeykoon, S. J. L. Billinge, E. Stach, J. Thomas, K. Guerrero, P. Munayco, J. Munayco, R. B. Scorzelli, P. Burnham, A. J. Viescas and S. S. Wong, *Chem. Mater.*, 2015, **27**, 3572–3592.
164 F. L. Deepak, M. Bañobre-López, E. Carbó-Argibay, M. F. Cerqueira, Y. Piñeiro-Redondo, J. Rivas, C. M. Thompson, S. Kamali, C. Rodríguez-Abreu, K. Kovnir and Y. V. Kolen'ko, *J. Phys. Chem. C*, 2015, **119**, 11947–11957.
165 S. R. Cooper, R. O. Candler, A. G. Cosby, D. W. Johnson, K. M. Ø. Jensen and J. E. Hutchison, *ACS Nano*, 2020, DOI: 10.1021/acsnano.9b09551.
166 F. M. Michel, L. Ehm, S. M. Antao, P. L. Lee, P. J. Chupas, G. Liu, D. R. Strongin, M. A. A. Schoonen, B. L. Phillips and J. B. Parise, *Science*, 2007, **316**, 1726–1729.
167 R. Harrington, D. B. Hausner, W. Xu, N. Bhandari, F. M. Michel, G. E. Brown, D. R. Strongin and J. B. Parise, *Environ. Sci. Technol.*, 2011, **45**, 9883–9890.
168 F. M. Michel, V. Barrón, J. Torrent, M. P. Morales, C. J. Serna, J.-F. Boily, Q. Liu, A. Ambrosini, A. C. Cismasu and G. E. Brown, *Proc. Natl. Acad. Sci. U. S. A.*, 2010, **107**, 2787–2792.
169 J. B. Parise, B. Xia, J. W. Simonson, W. R. Woerner, A. M. Plonka, B. L. Phillips and L. Ehm, *Crystals*, 2019, **9**, 246.
170 N. P. Funnell, M. F. Fulford, S. Inoué, K. Kletetschka, F. M. Michel and A. L. Goodwin, *Commun. Chem.*, 2020, **3**, 22.
171 A. I. Nguyen, K. M. Van Allsburg, M. W. Terban, M. Bajdich, J. Oktawiec, J. Amtawong, M. S. Ziegler, J. P. Dombrowski, K. V. Lakshmi, W. S. Drisdell, J. Yano, S. J. L. Billinge and T. D. Tilley, *Proc. Natl. Acad. Sci. U. S. A.*, 2019, **116**, 11630–11639.
172 J. Huang, J. D. Blakemore, D. Fazi, O. Kokhan, N. D. Schley, R. H. Crabtree, G. W. Brudvig and D. M. Tiede, *Phys. Chem. Chem. Phys.*, 2014, **16**, 1814–1819.
173 A. S. Batchellor, G. Kwon, F. A. L. Laskowski, D. M. Tiede and S. W. Boettcher, *J. Phys. Chem. C*, 2017, **121**, 25421–25429.
174 M. D. Donakowski, A. N. Mansour, I. R. Pala, C. N. Chervin, P. A. DeSario, J. W. Long and D. R. Rolison, *J. Phys. Chem. C*, 2018, **122**, 28895–28900.
175 P. Du, O. Kokhan, K. W. Chapman, P. J. Chupas and D. M. Tiede, *J. Am. Chem. Soc.*, 2012, **134**, 11096–11099.
176 M. W. Kanan, J. Yano, Y. Surendranath, M. Dincă, V. K. Yachandra and D. G. Nocera, *J. Am. Chem. Soc.*, 2010, **132**, 13692–13701.
177 X. Chen and A. Selloni, *Chem. Rev.*, 2014, **114**, 9281–9282.
178 X. Chen and S. S. Mao, *Chem. Rev.*, 2007, **107**, 2891–2959.
179 N. Lock, E. M. L. Jensen, J. L. Mi, A. Mamakhel, K. Noren, Q. B. Meng and B. B. Iversen, *Dalton Trans.*, 2013, **42**, 9555–9564.
180 W. Li, D. Corradini, M. Body, C. Legein, M. Salanne, J. Ma, K. W. Chapman, P. J. Chupas, A.-L. Rollet, C. Julien, K. Zhagib, M. Duttine, A. Demourgues, H. Groult and D. Dambournet, *Chem. Mater.*, 2015, **27**, 5014–5019.
181 W. Li, M. Body, C. Legein, O. J. Borkiewicz and D. Dambournet, *Inorg. Chem.*, 2016, **55**, 7182–7187.
182 W. Li, M. Body, C. Legein, O. J. Borkiewicz and D. Dambournet, *Eur. J. Inorg. Chem.*, 2017, 192–197.
183 J.-L. Mi, K. M. Ø. Jensen, C. Tyrsted, M. Bremholm and B. B. Iversen, *CrystEngComm*, 2015, **17**, 6868–6877.
184 S. Banerjee, A. Zangiabadi, A. Mahdavi-Shakib, S. Husremovic, B. G. Frederick, K. Barmak, R. N. Austin

and S. J. L. Billinge, *ACS Appl. Nano Mater.*, 2019, **2**, 6268–6276.
185 H. Zhang and J. F. Banfield, *Chem. Rev.*, 2014, **114**, 9613–9644.
186 X. Hua, Z. Liu, P. G. Bruce and C. P. Grey, *J. Am. Chem. Soc.*, 2015, **137**, 13612–13623.
187 C. L. Farrow, C. Shi, P. Juhas, X. Peng and S. J. L. Billinge, *J. Appl. Crystallogr.*, 2014, **47**, 561–565.
188 P. J. Chupas, K. W. Chapman and G. J. Halder, *J. Am. Chem. Soc.*, 2011, **133**, 8522–8524.
189 C. M. van Genuchten and J. Pena, *Environ. Sci.: Processes Impacts*, 2016, **18**, 1030–1041.
190 W. Li, R. Harrington, Y. Tang, J. D. Kubicki, M. Aryanpour, R. J. Reeder, J. B. Parise and B. L. Phillips, *Environ. Sci. Technol.*, 2011, **45**, 9687–9692.
191 C. M. van Genuchten and J. Peña, *Chem. Geol.*, 2016, **429**, 1–9.
192 M. H. Han, E. Gonzalo, G. Singh and T. Rojo, *Energy Environ. Sci.*, 2015, **8**, 81–102.
193 N. A. Chernova, M. Roppolo, A. C. Dillon and M. S. Whittingham, *J. Mater. Chem.*, 2009, **19**, 2526–2552.
194 M. P. Browne, Z. Sofer and M. Pumera, *Energy Environ. Sci.*, 2019, **12**, 41–58.
195 W. He, K. Ai, X. Ren, S. Wang and L. Lu, *J. Mater. Chem. A*, 2017, **5**, 19593–19606.
196 R. Uppuluri, A. Sen Gupta, A. S. Rosas and T. E. Mallouk, *Chem. Soc. Rev.*, 2018, **47**, 2401–2430.
197 D. S. Charles, M. Feygenson, K. Page, J. Neuefeind, W. Xu and X. Teng, *Nat. Commun.*, 2017, **8**, 15520.
198 B. Song, M. Tang, E. Hu, O. J. Borkiewicz, K. M. Wiaderek, Y. Zhang, N. D. Phillip, X. Liu, Z. Shadike, C. Li, L. Song, Y.-Y. Hu, M. Chi, G. M. Veith, X.-Q. Yang, J. Liu, J. Nanda, K. Page and A. Huq, *Chem. Mater.*, 2019, **31**, 3756–3765.
199 J. Liu, L. Yu, E. Hu, B. S. Guiton, X.-Q. Yang and K. Page, *Inorg. Chem.*, 2018, **57**, 6873–6882.
200 M. S. Hvid, H. S. Jeppesen, M. Miola, P. Lamagni, R. Su, K. M. Ø. Jensen and N. Lock, *IUCrJ*, 2019, **6**, 804–814.
201 P. Gao, P. Metz, T. Hey, Y. Gong, D. Liu, D. D. Edwards, J. Y. Howe, R. Huang and S. T. Misture, *Nat. Commun.*, 2017, **8**, 14559.
202 P. C. Metz, R. Koch and S. T. Misture, *J. Appl. Crystallogr.*, 2018, **51**, 1437–1444.
203 H. L. Andersen, K. M. Ø. Jensen, C. Tyrsted, E. D. Bøjesen and M. Christensen, *Cryst. Growth Des.*, 2014, **14**, 1307–1313.
204 K. J. Gross, S. Guthrie, S. Takara and G. Thomas, *J. Alloys Compd.*, 2000, **297**, 270–281.
205 T. Ressler, R. E. Jentoft, J. Wienold, M. M. Günter and O. Timpe, *J. Phys. Chem. B*, 2000, **104**, 6360–6370.
206 P. Norby, *J. Am. Chem. Soc.*, 1997, **119**, 5215–5221.
207 K. M. Ø. Jensen, M. Christensen, P. Juhas, C. Tyrsted, E. D. Bøjesen, N. Lock, S. J. L. Billinge and B. B. Iversen, *J. Am. Chem. Soc.*, 2012, **134**, 6785–6792.
208 C. Tyrsted, K. M. Ø. Jensen, E. D. Bøjesen, N. Lock, M. Christensen, S. J. L. Billinge and B. B. Iversen, *Angew. Chem., Int. Ed.*, 2012, **51**, 9030–9033.
209 C. Tyrsted, N. Lock, K. M. Ø. Jensen, M. Christensen, E. D. Bojesen, H. Emerich, G. Vaughan, S. J. L. Billinge and B. B. Iversen, *IUCrJ*, 2014, **1**, 165–171.
210 K. M. Ø. Jensen, H. L. Andersen, C. Tyrsted, E. D. Bøjesen, A.-C. Dippel, N. Lock, S. J. L. Billinge, B. B. Iversen and M. Christensen, *ACS Nano*, 2014, **8**, 10704–10714.
211 C. E. White, K. Page, N. J. Henson and J. L. Provis, *Appl. Clay Sci.*, 2013, **73**, 17–25.
212 D. Saha, E. D. Bojesen, K. M. Ø. Jensen, A. C. Dippel and B. B. Iversen, *J. Phys. Chem. C*, 2015, **119**, 13357–13362.
213 S. Birgisson, D. Saha and B. B. Iversen, *Cryst. Growth Des.*, 2018, **18**, 827–838.
214 D. Saha, K. M. Ø. Jensen, C. Tyrsted, E. D. Bojesen, A. H. Mamakhel, A. C. Dippel, M. Christensen and B. B. Iversen, *Angew. Chem., Int. Ed.*, 2014, **53**, 3667–3670.
215 S. Sommer, I. G. Nielsen and B. B. Iversen, *Chem.–Eur. J.*, 2020, **26**, 1–6.
216 M. Juelsholt, T. Lindahl Christiansen and K. M. Ø. Jensen, *J. Phys. Chem. C*, 2019, **123**, 5110–5119.
217 H. Xu, S. Sommer, N. L. N. Broge, J. Gao and B. B. Iversen, *Chem.–Eur. J.*, 2019, **25**, 2051–2058.
218 E. D. Bøjesen, K. M. Ø. Jensen, C. Tyrsted, A. Mamakhel, H. L. Andersen, H. Reardon, J. Chevalier, A.-C. Dippel and B. B. Iversen, *Chem. Sci.*, 2016, **7**, 6394–6406.
219 N. L. N. Broge, F. Søndergaard-Pedersen, S. Sommer and B. B. Iversen, *Adv. Funct. Mater.*, 2019, **29**, 1902214.
220 L. Soderholm and J. F. Mitchell, *APL Mater.*, 2016, **4**, 053212.
221 C. K. Christensen, M. A. H. Mamakhel, A. R. Balakrishna, B. B. Iversen, Y.-M. Chiang and D. B. Ravnsbæk, *Nanoscale*, 2019, **11**, 12347–12357.
222 X. Hua, Z. Liu, M. G. Fischer, O. Borkiewicz, P. J. Chupas, K. W. Chapman, U. Steiner, P. G. Bruce and C. P. Grey, *J. Am. Chem. Soc.*, 2017, **139**, 13330–13341.
223 Y.-Y. Hu, Z. Liu, K.-W. Nam, O. J. Borkiewicz, J. Cheng, X. Hua, M. T. Dunstan, X. Yu, K. M. Wiaderek, L.-S. Du, K. W. Chapman, P. J. Chupas, X.-Q. Yang and C. P. Grey, *Nat. Mater.*, 2013, **12**, 1130–1136.
224 T. Koketsu, J. Ma, B. J. Morgan, M. Body, C. Legein, W. Dachraoui, M. Giannini, A. Demortière, M. Salanne, F. Dardoize, H. Groult, O. J. Borkiewicz, K. W. Chapman, P. Strasser and D. Dambournet, *Nat. Mater.*, 2017, **16**, 1142–1148.
225 S.-K. Jung, I. Hwang, D. Chang, K.-Y. Park, S. J. Kim, W. M. Seong, D. Eum, J. Park, B. Kim, J. Kim, J. H. Heo and K. Kang, *Chem. Rev.*, 2019, DOI: 10.1021/acs.chemrev.9b00405.
226 B. Shyam, K. W. Chapman, M. Balasubramanian, R. J. Klingler, G. Srajer and P. J. Chupas, *Angew. Chem., Int. Ed.*, 2012, **51**, 4852–4855.
227 K. M. Wiaderek, O. J. Borkiewicz, E. Castillo-Martínez, R. Robert, N. Pereira, G. G. Amatucci, C. P. Grey, P. J. Chupas and K. W. Chapman, *J. Am. Chem. Soc.*, 2013, **135**, 4070–4078.
228 C. Henriksen, J. K. Mathiesen, Y.-M. Chiang, K. M. Ø. Jensen and D. B. Ravnsbæk, *ACS Appl. Energy Mater.*, 2019, **2**, 8060–8067.

229 C. K. Christensen, D. R. Sørensen, J. Hvam and D. B. Ravnsbæk, *Chem. Mater.*, 2019, **31**, 512–520.
230 J. J. Choi, X. H. Yang, Z. M. Norman, S. J. L. Billinge and J. S. Owen, *Nano Lett.*, 2014, **14**, 127–133.
231 P. Cottingham and R. L. Brutchey, *Chem. Mater.*, 2016, **28**, 7574–7577.
232 C. Shi, S. J. L. Billinge, E. Puma, S. H. Bang, N. J. H. Bean, J.-C. de Sugny, R. G. Gambee, R. C. Haskell, A. Hightower and T. C. Monson, *Phys. Rev. B: Condens. Matter Mater. Phys.*, 2018, **98**, 085421.
233 K. T. Dissanayake and F. A. Rabuffetti, *Chem. Mater.*, 2018, **30**, 2453–2462.
234 L. Ehm, F. M. Michel, S. M. Antao, C. D. Martin, P. L. Lee, S. D. Shastri, P. J. Chupas and J. B. Parise, *J. Appl. Crystallogr.*, 2009, **42**, 15–21.
235 F. M. Michel, S. M. Antao, P. J. Chupas, P. L. Lee, J. B. Parise and M. A. A. Schoonen, *Chem. Mater.*, 2005, **17**, 6246–6255.
236 J. B. Parise, L. Ehm, F. M. Michel, S. Antao, P. J. Chupas, P. L. Lee, C. D. Martin and S. Shastri, *AIP Conf. Proc.*, 2009, **1092**, 41–44.
237 M. Feygenson, J. C. Neuefeind, T. A. Tyson, N. Schieber and W.-Q. Han, *Inorg. Chem.*, 2015, **54**, 11226–11235.
238 K. Page, J. Li, R. Savinelli, H. N. Szumila, J. Zhang, J. K. Stalick, T. Proffen, S. L. Scott and R. Seshadri, *Solid State Sci.*, 2008, **10**, 1499–1510.
239 C. Shi, M. Beidaghi, M. Naguib, O. Mashtalir, Y. Gogotsi and S. J. L. Billinge, *Phys. Rev. Lett.*, 2014, **112**, 125501.
240 H.-W. Wang, M. Naguib, K. Page, D. J. Wesolowski and Y. Gogotsi, *Chem. Mater.*, 2016, **28**, 349–359.
241 X. Xiao, P. Urbankowski, K. Hantanasirisakul, Y. Yang, S. Sasaki, L. Yang, C. Chen, H. Wang, L. Miao, S. H. Tolbert, S. J. L. Billinge, H. D. Abruña, S. J. May and Y. Gogotsi, *Adv. Funct. Mater.*, 2019, **29**, 1809001.
242 M. W. Terban, C. Shi, R. Silbernagel, A. Clearfield and S. J. L. Billinge, *Inorg. Chem.*, 2017, **56**, 8837–8846.
243 M. Eremenko, V. Krayzman, A. Gagin and I. Levin, *J. Appl. Crystallogr.*, 2017, **50**, 1561–1570.
244 A. Gagin, A. J. Allen and I. Levin, *J. Appl. Crystallogr.*, 2014, **47**, 619–629.
245 V. Krayzman, I. Levin and M. G. Tucker, *J. Appl. Crystallogr.*, 2008, **41**, 705–714.
246 H. N. Bordallo, C. Lioma, J. Taylor and D. N. Argyriou, *IUCrJ*, 2020, **7**, 1–2.
247 H. S. Geddes, H. Blade, J. F. McCabe, L. P. Hughes and A. L. Goodwin, *Chem. Commun.*, 2019, **55**, 13346–13349.
248 K. W. Chapman, S. H. Lapidus and P. J. Chupas, *J. Appl. Crystallogr.*, 2015, **48**, 1619–1626.
249 J. M. Cole, X. Cheng and M. C. Payne, *Inorg. Chem.*, 2016, **55**, 10870–10880.
250 D. Olds, P. F. Peterson, M. K. Crawford, J. R. Neilson, H.-W. Wang, P. S. Whitfield and K. Page, *J. Appl. Crystallogr.*, 2017, **50**, 1744–1753.
251 C.-H. Liu, Y. Tao, D. Hsu, Q. Du and S. J. L. Billinge, *Acta Crystallogr., Sect. A: Found. Adv.*, 2019, **75**, 633–643.
252 R. Gu, S. Banerjee, Q. Du and S. J. L. Billinge, *Acta Crystallogr., Sect. A: Found. Adv.*, 2019, **75**, 658–668.
253 L. Yang, P. Juhás, M. W. Terban and S. J. L. Billinge, *Acta Crystallogr., Sect. A: Found. Adv.*, 2020, **76**, 395–409.